GCA Technical Report No. 64-4-N

THE METEOROLOGY OF MARS AND VENUS

FINAL REPORT

George Ohring
Edward M. Brooks
Joseph Mariano

March 1964

Contract No. NASw-704

Prepared for

NATIONAL AERONAUTICS AND SPACE ADMINISTRATION
WASHINGTON 25, D. C.

GEOPHYSICS CORPORATION OF AMERICA
Bedford, Massachusetts

ABSTRACT

27238

Studies are performed on the meteorology of the planets Mars and Venus.

MARS

A thermodynamic diagram for the Martian atmosphere is constructed. The diagram is based upon a model atmosphere, consisting of 83% nitrogen, 11% carbon dioxide, and 6% argon, with a surface pressure of 25 mb. Lines of constant pressure, temperature, potential temperature, wet-bulb potential temperature, and saturation specific humidity are included on the diagram.

A theoretical study of tides in the Martian atmosphere indicates that tidal motions are not likely to play any significant role in Martian meteorology.

An estimate of the annual radiation budget reveals that below latitude 35^{o} there is a surplus of radiational energy, and above 35^{o} there is a deficit. For balance to occur, the average heat transport across 35^{o} latitude is about 0.5×10^{16} cal min^{-1}. This is an order of magnitude less than the transport required on the Earth.

VENUS

Improved greenhouse models for the Venus atmosphere are developed and discussed. A two-layer greenhouse model, consisting of a troposphere with arbitrary but constant lapse-rate of temperature, and an isothermal stratosphere in gross radiative equilibrium, is applied to Venus, Mars, and Earth. For Venus, the computations indicate that the observed high surface temperatures can be the result of a strong greenhouse effect due to an infrared-opaque cloud high in the Venus atmosphere and carbon dioxide or other infrared absorbers in the atmosphere.

Estimates of the amount of solar radiation absorbed by carbon dioxide in the Venus atmosphere indicate that about 12% of the solar radiation (after albedo losses) is absorbed by carbon dioxide's near infrared bands.

On the basis of infrared radiative equilibrium, the temperature variation with altitude in the layer between the Venus surface and cloud-base is determined.

TABLE OF CONTENTS

SECTION 1

INTRODUCTION

This Final Report covers research performed during the past year on the Meteorology of Mars and Venus under NASA Contract No. NASw-704. The goal of this research is to increase knowledge about these planets through a synthesis of available observations with appropriate meteorological theory.

Although the number of useful observations of planetary atmospheric characteristics is extremely small compared to the number of observations available for the Earth's atmosphere, it is increasing at an accelerated rate. Proper analysis and interpretation of these observations in the light of appropriate theory is of the utmost importance in achieving the objectives of adequate understanding of planetary atmospheres, proper planning of future observations of planetary atmospheres, and proper design of space vehicles that will enter planetary atmospheres. It is realized that the results of such research are subject to change as more and more observational data become available. But these results represent the best possible estimates of conditions and processes on these planets, and, although uncertain in some respects, they still are extremely useful for achieving the above objectives.

During the year a number of topics bearing on the meteorology of Mars and Venus were studied. For some of these topics, technical reports and articles for scientific journals have been prepared; for these topics, only a summary of the research is reported in this report. In the case of the remaining topics, detailed discussions are presented in this report.

Research on Mars included studies of tides in the atmosphere, thermodynamic diagrams, and the annual radiation budget of the planet. Research on Venus included studies of surface and atmospheric temperatures, and greenhouse models. These research studies are discussed in the remainder of this report.

SECTION 2

METEOROLOGY OF MARS

2.1 THERMODYNAMIC DIAGRAMS FOR THE MARTIAN ATMOSPHERE

2.1.1 Introduction. The general purpose of thermodynamic diagrams is to delineate changes of temperature resulting from compression or expansion of atmospheric parcels when the state of one constituent changes. For the temperatures and pressures of the atmospheres of the Earth and Mars, water may experience three phases, and carbon dioxide, two. Although water and carbon dioxide represent only small fractions of the atmospheres of the Earth and Mars, they are important because of their temperature effects through phase changes and also through their absorption and emission of electromagnetic radiation. Water is the substance chosen for adiabatic charts of the Earth's atmosphere, and it is used for similar diagrams of Mars' atmosphere (an example of which is presented in this report).

The Mars diagram is patterned after a pseudo-adiabatic diagram for the Earth. The contents and uses of the latter will now be summarized. The coordinates include some function of pressure, serving as an approximate height scale, for the ordinate, and temperature for the abscissa.

Other parameters are represented by isopleths of mixing ratio at water saturation, potential temperature (dry adiabats), and wet-bulb potential temperature or equivalent potential temperature (saturation adiabats). For a given vertical distribution of pressure, temperature, and relative humidity, a great deal of information can be obtained with the aid of an adiabatic chart. For each level of the distribution the following quantities can be found: black-body radiation, saturation vapor pressure, actual vapor pressure, mixing ratio or specific humidity, dew point, pressure and temperature at the lifting condensation level, wet-bulb temperature, equivalent temperature, and approximate height above sea level. An analysis of the entire vertical distribution can yield the following elements: thermal stability indices, distribution and amounts of positive energy available for convection and negative energy, or work to be done by forced uplift, pressures and temperatures at the convection condensation level and at the level of free convection, convection temperature, air mass identification, pressures and temperatures at a front aloft and at the tropopause, approximate height of the base of a subsidence layer and the thickness of a turbulence layer, etc. (Most of these elements are defined in meteorology textbooks, such as Holmboe, Forsythe, and Gustin, 1945.)

The composition and pressure of the Martian atmosphere must be specified before curves can be drawn to make an adiabatic diagram for Mars. Since the concentrations of the atmospheric gases and the mean surface pressure are not accurately known, model atmospheres must be assumed.

Some diagrams were based on a model by Grandjean and Goody, which indicated 2% carbon dioxide by volume and the remaining 98% consisting of mostly nitrogen plus traces of other constituents, including water, for a surface pressure of 85 mb. Another diagram was prepared for the same concentrations, but with 20 mb pressure at the surface. The diagram presented in this report is based on "assumption b," a new model by Kaplan, Münch, and Spinrad (1964), which calls for a surface pressure of 25 mb, based on measurements of CO_2 bands near 8700 Å and 2μ. This pressure consists of partial pressures equal to 19 mb of nitrogen, 4 mb of carbon dioxide, and 2 mb of argon 40, plus traces of other components, including a total precipitable water content of only 14μ. This assumption was chosen because Kaplan et al. preferred it to their "assumption a," which specifies primarily an argon atmosphere by interchanging the partial pressures of nitrogen and argon.

The accompanying table of the important thermodynamic constants gives a comparison between the "assumption b" atmosphere of Mars and dry air of the Earth's atmosphere. All of the listed constants except the molecular weight are smaller for Mars than for Earth. However, none of the constants for Mars and Earth differ by more than 5% except the acceleration of gravity. Hence, a diagram for the Martian atmosphere can be made quite similar to the adiabatic diagram for the Earth's atmosphere.

The surface pressure on Mars is still not known with any precision. Although the accompanying diagram is based on 25 mb, a recent measurement of the 1.67μ CO_2 band led Kuiper to propose the value of 10 mb (GCA, 1964).

Table 2.1

Comparison of thermodynamic constants for atmospheres of Mars and Earth.

Constant	Symbol	Earth "Dry Air"	Mars Atmosphere "Assumption b"	Mars-Earth / Earth
Molecular weight	m	28.97	30.52	+ 5%
Specific gas constant	$R(\text{cal gm}^{-1}\text{deg}^{-1})$	0.0686	0.0652	- 5%
Specific heat at constant pressure	$c_p(\text{cal gm}^{-1}\text{deg}^{-1})$	0.240	0.231	- 4%
Specific heat at constant volume	$c_v(\text{cal gm}^{-1}\text{deg}^{-1})$	0.171	0.166	- 3%
Acceleration of gravity	$g(\text{m sec}^{-2})$	9.80	3.76	- 62%
Poisson constants	$\eta = c_p/c_v$	1.400	1.393	- 0.5%
	$\kappa = R/c_p$	0.286	0.282	- 1%
Ratio of molecular weights of water and atmosphere	$\epsilon = m_v/m$	0.622	0.590	- 5%

2.1.2 Representation of Quantities on the Mars Diagram. A brief legend identifies the curves drawn on the accompanying thermodynamic diagram, Figure 2.1, for the Martian atmosphere.

The ordinate is chosen as $-\log\left(\frac{p}{p_0}\right)$ to represent a scale of approximate height above the surface, as suggested by the hypsometric formula,

$$z = -\frac{R}{g} T_m \ell n \left(\frac{p}{p_0}\right)$$

where z is the height above the surface of Mars, R is the specific gas constant, g is the acceleration of gravity, and T_m is the mean virtual temperature between the levels defined by p, the pressure, and p_0, the surface pressure. Since clouds, perhaps of water or ice, have been observed at a height of about 30 km, where $\frac{p}{p_0}$ is approximately 0.1, the ordinate is extended through two logarithm cycles to the base 10. The corresponding pressure ranges from 25 mb to ¼ mb. Scales of $\frac{p}{p_0}$ and of p are supplied on the diagram's right and left margins, respectively.

The abscissa is a linear scale of temperature, with values labeled in ^{o}C at the top of the diagram and in both ^{o}K and ^{o}C at the bottom. The temperature range in the diagram is from + 30^{o}C (303^{o}K) down to - 150^{o}C (123^{o}K) to accommodate the low temperatures of the Martian atmosphere. Since black-body radiation, E, is a function of temperature only, the corresponding values of E could also be labeled along the T scale in accordance with the formula,

$$E = \sigma T^4 ,$$

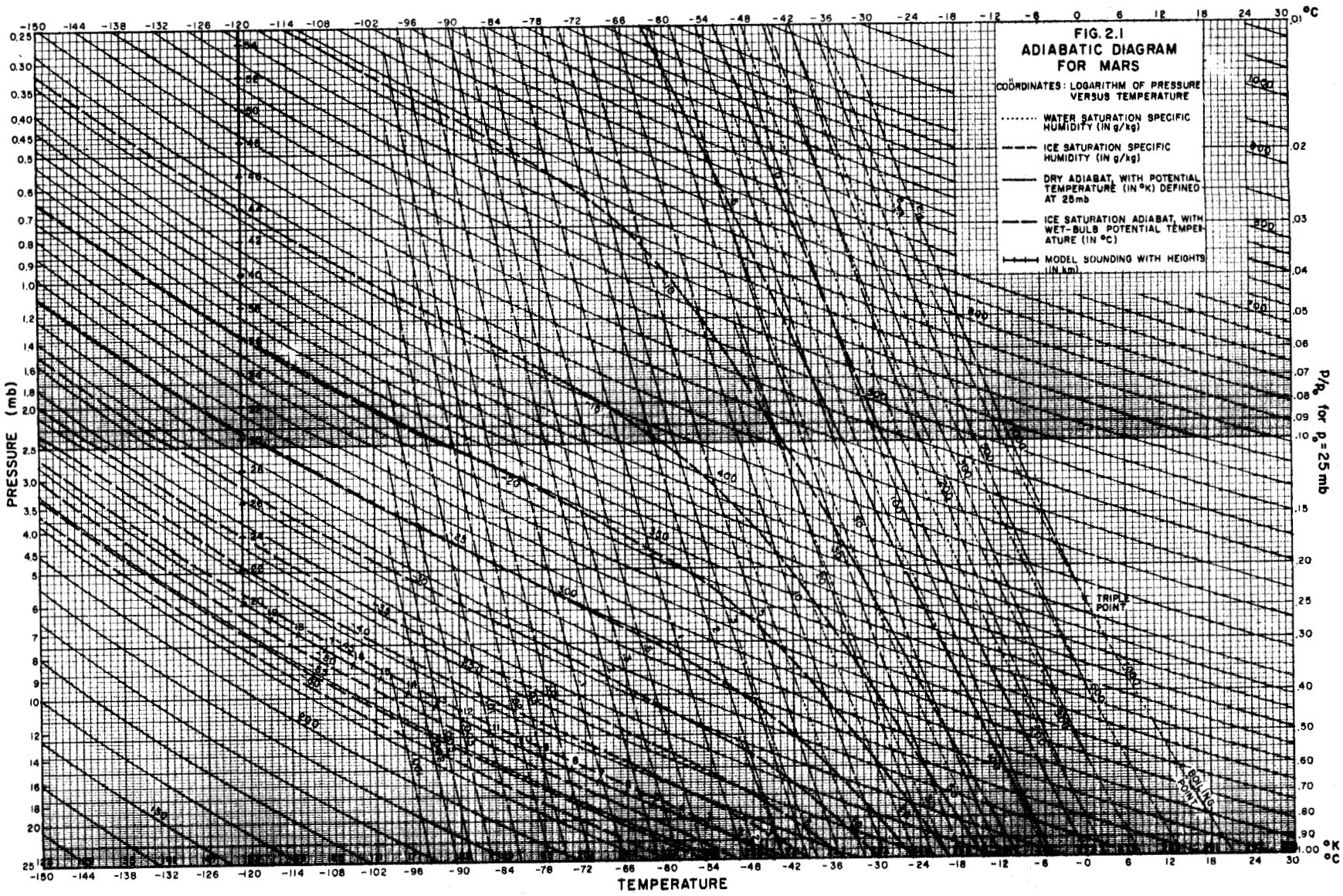
FIG. 2.1
ADIABATIC DIAGRAM
FOR MARS
COORDINATES: LOGARITHM OF PRESSURE VERSUS TEMPERATURE
WATER SATURATION SPECIFIC HUMIDITY (IN g/kg)
ICE SATURATION SPECIFIC HUMIDITY (IN g/kg)
DRY ADIABAT, WITH POTENTIAL TEMPERATURE (IN °K) DEFINED AT 25mb
ICE SATURATION ADIABAT, WITH WET-BULB POTENTIAL TEMPERATURE (IN °C)
MODEL SOUNDING WITH HEIGHTS (IN km)
TRIPLE POINT
BOILING POINT
PRESSURE (mb)
TEMPERATURE
p/p_s for p_s = 25 mb
°K
°C

where σ is the Stefan-Boltzmann constant. An advantage of plotting this diagram on semi-log paper is that it yields an area, $\oint T\, d\left[\log\left(\frac{p}{p_0}\right)\right]$, strictly proportional to thermodynamic energy or work.

The first set of curves to be discussed are needed on the diagram to represent the amount of water vapor for saturation with respect to water. Due to the low pressures on Mars, the saturation specific humidities, q_{ws}, at the higher temperatures cannot be approximated by the saturation mixing ratios, w_{ws} (an approximation used for the Earth's atmosphere). This derives from the fact that as the saturation vapor pressure, e_{ws}, approaches the total pressure, p, the saturation specific humidity approaches unity whereas the saturation mixing ratio increases without limit as its denominator approaches zero. For the purpose of deriving saturation adiabats later, the saturation specific humidity was chosen for isopleth construction (because the process refers to a unit mass of air, including the vapor). Since specific humidity determines mixing ratio uniquely, the isopleths could be labeled in terms of saturation mixing ratios if desired.

The procedure was to choose values of q_{ws} equal to 1, 2, 3, 5, and 10 times 10^0, 10^1, and 10^2 g/kg (rather evenly spaced logarithms of q_s to give a roughly uniform increase of T). The e_{ws} was computed from the formula

$$e_{ws} = p\left[\left(\epsilon/q_{ws}\right) + \left(1 - \epsilon\right)\right]^{-1},$$

where $\epsilon = m_v/m = 0.590$. The corresponding values of T were looked up (List, 1958, Table 94), tabulated, and plotted against p for each chosen q_{ws} value. Temperatures were used down to the lower limit of the table, - 50°C, to cover the possibility of supercooled water clouds, which are known to occur at the same temperatures in the Earth's atmosphere. The correction factor, f_w (List, 1958, Table 89), was omitted because its departure from unity was less than percentage errors arising from an inexact model atmosphere. The curves of q_{ws} give the dew point changes with adiabatic pressure changes. The last curve on the right represents the case of saturation vapor pressure e_{ws} equal to the total pressure, p. Hence, it is a curve of T versus e_{ws} (read on the p scale), and T is the boiling point. The low pressure on Mars makes the boiling point low. Starting at 21.1°C for 25 mb (the surface), it drops to 0°C for 6.1 mb (at about 20 km), the "triple point," where all three phases of water can exist in equilibrium. For temperatures above the boiling point, no saturation and presumably no water clouds can occur, since

$$e \leq p < e_{ws}, \text{ or } \frac{e}{e_{ws}} < 100\%,$$

where e is the ambient vapor pressure. Because of the small water vapor concentrations on Mars, it is doubtful if there is enough to produce water clouds at any temperature (above - 50°C).

The second set of curves for the diagram represent q_{is}, the saturation specific humidity with respect to ice. These curves were made to overlap the first set of curves, for q_{ws}, in the temperature range from

- 50°C up to 0°C, where either ice or supercooled water clouds could occur. The low temperatures in the Martian atmosphere justify the extension of the ice saturation data to - 100°C on the diagram. Because of the large range in temperature, q_{is} values run the gamut from 10^{-3} to 10^{+3} g/kg, the latter giving T versus e_{is}, the ice saturation vapor pressure. The q_{is} lines were prepared in the same way as the q_{ws} lines: by use of the formula,

$$e_{is} = p \left[\left(\epsilon / q_{is} \right) + \left(1 - \epsilon \right) \right]^{-1} .$$

Tables were used as before (List, 1958, Table 96), and the f_i factor (List, 1958, Table 90) was rounded off to unity. For a given T < 0°C, a q_{is} curve appears higher on the diagram, or at a lower pressure, than the q_{ws} curve of the same value because

$$e_{is} < e_{ws} \text{ for } T < 0^{\circ}C .$$

However, the q_{is} curve meets its corresponding q_{ws} curve at T = 0°C and ends there, since ice cannot have a temperature greater than 0°C. The q_{is} curves give the frost point in terms of pressure for dry adiabatic processes.

The next set of curves represents the dry adiabats, which give the relation between T and p for adiabatic processes without sublimation, condensation, or evaporation, namely at constant potential temperature, θ:

$$\frac{T}{\theta} = \left(\frac{p}{p_0} \right)^{\kappa} , \quad \kappa = \frac{R}{c_p} ,$$

where R is the specific gas constant for the atmospheric mixture and c_p is the specific heat at constant pressure. Since $\kappa = 0.282$ for the selected model atmosphere of Mars, it can be approximated by $\kappa = \frac{2}{7}$, the same exponent used for dry adiabats for the Earth's atmosphere. Since θ is defined as the temperature of air reduced dry adiabatically from pressure p to pressure p_0, θ on the Mars diagram is the same as θ on the Earth only if p_0 = 1000 mb. Hence, the dry adiabats on the Earth's adiabatic chart may be used without any modification on a Mars diagram. However, it was considered more appropriate to define p_0 as 25 mb in the accompanying diagram. Regardless of what value of p_0 is selected, the dry adiabats and their labels are not affected as long as the ordinate scale labeled p/p_0 is used (right margin) and if p_0 is the reference pressure for the definition of θ. The dry adiabats were drawn for $10K^o$ intervals for $130^oK \leq \theta \leq 400^oK$, $20K^o$ for $400^oK \leq \theta \leq 800^oK$, and $50K^o$ for $800^oK \leq \theta \leq 1100^oK$. Since the dry adiabats are not straight lines on this semi-log diagram, they were drawn originally on log-log paper as straight lines and then transposed point by point to save the trouble of computing a lot of points.

The final set of curves represents the ice saturation adiabats: curves of constant wet-bulb potential temperature, θ_w, or curves of constant equivalent potential temperature, θ_e. They show the temperature changes when adiabatic pressure changes cause sublimation, with the release or consumption of the latent heat of sublimation reducing the dry adiabatic temperature changes. Sublimation was chosen instead of

condensation, used on Earth diagrams, because of the lower temperatures in the Martian atmosphere. The ice saturation adiabats were constructed from the approximation formula,

$$(dT)_p = -\frac{L_i}{c_p} dq_{is} \quad ,$$

where $(dT)_p$ is the isobaric temperature increase resulting from a decrease of $-dq_{is}$ in saturation specific humidity with sublimation. The ratio, L_i/c_p on Mars is 2.93 and 2.94 x 10^3 C^o at 0 and - 53°C, respectively. For ease in computation, the value of $3x10^3C^o$ was chosen. This means that for every 1 g/kg sublimated, there is a temperature rise of $3C^o$ above the temperature of the dry adiabat. To allow for the differences in slope of the dry adiabats, half of the temperature rise was applied at the bottom of a layer and the other half at the top of the layer, the thickness of which is defined by a given drop of ice saturation specific humidity. To be correctly drawn, the slope of each saturation adiabat had to be intermediate between the slopes of the saturation specific humidity curves and of the dry adiabats. At the higher temperatures, the saturation adiabats are nearly parallel to the humidity curves, but at low temperatures they become parallel to the dry adiabats, due to the very small amount of moisture available for sublimation even at saturation. Consequently, there is a marked divergence in the saturation adiabats, drawn for every $5C^o$ at 25 mb, but appearing farther apart (greater T difference) at lower pressures. The saturation adiabats are labeled in terms of equally spaced values of θ_w from -60°C to 0°C, rather than in θ_e, whose intervals between successive values rapidly increase with T.

The four sets of curves for the Mars diagram described above are quite similar to the curves on the Earth diagrams. However, a big difference between the planets appears when the height scale for Mars is compared with the Earth's height scale because the gravity on Mars is only 38% of the Earth's gravity. (See accompanying Table 2.1) A model temperature variation with pressure was plotted on the Mars diagram. The surface temperature was assumed to be $230^{o}K$ ($-43^{o}C$). The lapse rate was assumed to be dry adiabatic up to a tropopause at an assumed height of 20 km, above which the Martian stratosphere was chosen to be isothermal. The dry adiabatic lapse rate for Mars is

$$\gamma_d = -\frac{dT}{dz} = \frac{g}{c_p} = 3.65\ K^{o}/km,$$

about 1/3 of that of the earth.

The temperature at $z \geq 20$ km in this hypothetical sounding is $152.2^{o}K$ ($-120.8^{o}C$). At 20 km, p/p_0 is .236. The formulas used for computing the pressures at chosen heights were

$$\left(\frac{p}{p_0}\right)^{\frac{2}{7}} = 1 - \frac{\gamma_d\, z}{T_0} = 1 - .01691\ z\ km^{-1} \text{ for } z \leq 20 \text{ km},$$

where the subscript 0 refers to the surface of Mars, and

$$\frac{p}{p_{20}} = \exp\left[-\frac{\gamma_d(z-20km)}{\kappa\, T_{20}}\right] = \exp\left[-.09067\ km^{-1}(z-20km)\right] \text{ for } z \geq 20 \text{ km},$$

where the subscript 20 refers to the 20-km level. The diagram shows that the height scale is nearly invariant for its entire range from the surface to about 55 km.

Future thermodynamic diagrams for Mars will improve as our knowledge of the Martian atmosphere increases.

2.2 TIDES IN THE ATMOSPHERE OF MARS

NOTE: The subject matter of this section has been treated in detail in the following technical report under the present contract.

Craig, Richard A., 1963: Tides in the Atmospheres of Earth and Mars. GCA Technical Report No.63-26-N, Contract NASw-704, 45 pp.

We present here the background and a summary of the reported work; for a complete discussion, consult the technical report.

The expression atmospheric tides is generally used to refer to atmospheric oscillations whose periods are equal to or sub-multiples of the solar or lunar day, regardless of whether the oscillations are gravitationally or thermally excited. The theory of tides in the Earth's atmosphere has a long history and has claimed the attention of such men as Laplace, Kelvin, Rayleigh, Margules, Lamb, Chapman, Taylor, and Pekeris. One reason for this interest in the relatively small oscillations involved is the rather surprising observation that in our atmosphere the solar semi-diurnal tide predominates over the lunar tide (with its stronger gravitational excitation) and the solar diurnal tide (with its stronger thermal excitation). Although all the details of this phenomenon are not clearly understood, it now appears that the predominance of solar tides over lunar is due to the importance of thermal excitation and that

the relative strength of the solar semi-diurnal oscillation results from a peculiar response of our atmosphere to the periodic heating. There is no reason to believe that the theory, which necessarily contains many simplifications, is inadequate and one may apply it with reasonable confidence to the atmospheres of other planets. The history and present status of tidal theory has been reviewed recently by Siebert (1961), to whose work the reader is referred for further details.

The planet Mars is one for which the application of tidal theory appears to have some interest. The relatively large diurnal temperature variation that is inferred for the surface of Mars raises the question of the response thereto of the Martian atmosphere. Both Mintz (1961) and Ohring and Cote' (1963) have speculated on the possibility of an important diurnal oscillation in the Martian atmosphere. The purpose of this research is to investigate such a possibility with the aid of standard tidal theory.

The theory leads to two ordinary differential equations, Laplace's tidal equation and the radial equation. Both contain a constant h, which arises in the separation of variables in an earlier partial differential equation.

In the study of tidal oscillations, one first specifies a period which is equal to or a submultiple of the solar day (in our atmosphere one is also interested in periods similarly related to the lunar day, but this has no application to Mars). For the specified period and a

specified wave number, Laplace's tidal equation has a series of solutions in the form of Hough's functions, with each of which is associated a particular value of h, called an equivalent depth. Each of these solutions is spoken of as a mode of oscillation and describes the latitudinal behavior of the oscillation. Because the ratio of the length of the solar day to the length of the sidereal day is essentially the same on Mars as on Earth, a given mode of oscillation has essentially the same form in the two atmospheres. On the other hand, the equivalent depth corresponding to a given mode of oscillation is less on Mars than on Earth because of differences in radius and mass of the planets.

In the case of free oscillations (not gravitationally or thermally forced), the radial equation is soluble for only one or two values of h, which are spoken of as eigenvalues. The number and magnitude of the eigenvalue(s) depend on the average vertical temperature distribution. The Earth's atmosphere has only one such eigenvalue with a value of about 10 km. The Earth's atmosphere would have a second eigenvalue of about 8 km if the temperature near the stratopause were as high as was once thought likely. The temperature distribution in the Martian atmosphere is not well known. The temperature is believed to decrease upward, more rapidly near the surface than at higher levels. For a model atmosphere embodying these features, the Martian atmosphere also has one eigenvalue of about 20 km. This value does not depend very critically on the exact temperatures that are assumed. A second eigenvalue might arise if the temperature distribution at still higher levels were of a rather special character, but this possibility has not been explored.

The importance of the eigenvalues in tidal theory is as follows: if an excited mode of oscillation happens to have an equivalent depth whose value is very close to one of the eigenvalues, then that mode will be greatly amplified by resonance effects. A comparison of the equivalent depths on Mars for modes that might be excited by solar heating with the eigenvalue inferred for the Martian atmosphere indicates that no resonance magnification is to be expected.

Tidal oscillations on Mars might arise from the rather large diurnal temperature variation near the surface that is inferred from theory and observation. This possibility has been considered, and it appears highly improbable that the amplitude of the resulting diurnal surface-pressure oscillation (relative to the total surface pressure) exceeds the amplitude of Earth's semi-diurnal oscillation. If this conclusion is correct, tidal oscillations arising from this cause are not likely to play any significant role in the Martian general circulation.

Tidal oscillations might also arise from diurnal or semi-diurnal temperature oscillations caused by periodic radiative processes occurring through deep layers of the Martian atmosphere. In our present state of knowledge about the composition of the Martian atmosphere, one cannot be sure about the amplitude of such temperature oscillations, but they are probably too small to excite significant tidal motions. If the atmosphere should contain ozone in amounts greater than now suspected (or any other gas that absorbs significant amounts of solar radiation), then this tentative conclusion would have to be re-examined.

Thus, in the context of present inferences about temperature and composition of the Martian atmosphere, there is no reason to expect that tidal motions play an important role in the meteorology of Mars.

2.3 ANNUAL RADIATION BUDGET FOR MARS

2.3.1 Introduction

Over the course of a year, the amount of solar radiation received by a planet is balanced by the amount of infrared radiation emitted by the planet. However, at any one time, or at any one location, incoming solar radiation does not, in general, equal outgoing infrared radiation. The large scale variations of the difference between incoming and outgoing radiation represent heat energy sources and sinks; these sources and sinks are the driving forces of the general circulation of a planetary atmosphere, and knowledge of their magnitude and distribution is a basic requirement for an understanding of planetary circulations.

The net incoming solar radiation at the top of the Martian atmosphere is solely a function of the solar constant, solar-Martian geometry, and Martian planetary albedo. The solar constant and the required geometry are well known; the Martian planetary albedo, and, in particular, its variations with latitude and season are known to a lesser degree of accuracy. The outgoing radiation depends upon the surface temperatures, and the composition and temperatures of the atmosphere. Both composition and temperature, especially variations with latitude, altitude, and season, are not known very well; however, there is sufficient information available to allow construction of atmospheric models that can be used for preliminary estimates of the radiation budget. In the present examination of the problem, we shall attempt to obtain a preliminary estimate of the annual radiation budget of Mars - the average variation

with latitude of incoming and outgoing radiation at the top of the Martian atmosphere.

2.3.2 Methodology.

The variation of incoming solar radiation with latitude at the top of the Martian atmosphere - before correction for albedo losses - was computed some time ago by Milankovitch (1920). These values are shown in column 2 of Table 2.2 and are based upon a solar constant of 2 cal cm^{-2} min^{-1} at the Earth's distance from the Sun. The variation of Martian planetary albedo with latitude has recently been estimated by Sagan (1964), and the average hemispheric variation is shown in Table 2.2. By multiplying the incoming solar radiation by (1 - A), where A is the albedo, one can obtain the latitudinal variation of net incoming radiation, which is the incoming part of the radiation budget.

To determine the outgoing radiation, knowledge is required of the mean latitudinal variation of surface temperature, of vertical distribution of temperature, and of atmospheric absorption characteristics. In the present model, the mean latitudinal variation of surface temperature is based upon Ohring et al's (1962) processing of Gifford's (1956) analysis of mid-day radiometric observations; this processing consisted of extrapolation of Gifford's temperature curves to the poles and correction for diurnal variations. These surface temperatures are shown in Table 2 2.

For the atmospheric temperatures and absorption characteristics, it is assumed that:

Table 2 2. Annual radiation budget of Mars.

Latitude deg	I_o cal $cm^{-2} min^{-1}$	A	$I_o(1 - A)$	T_g ^oK	F(o) cal $cm^{-2} min^{-1}$
0 - 10	0.262	0.200	0.209	238	0.194
10 - 20	.254	.185	.207	238	.194
20 - 30	.240	.178	.198	236	.187
30 - 40	.220	.185	.180	234	.181
40 - 50	.195	.180	.160	232	.175
50 - 60	.167	.160	.140	228	.163
60 - 70	.139	.150	.118	223	.149
70 - 80	.125	.165	.104	218	.136
80 - 90	.118	.185	.096	210	.118

1) The atmosphere consists of two layers: a troposphere, in which the temperature decreases with height at a rate of 0.9 times the adiabatic lapse rate, or about 3.3°K/km, and a stratosphere, in which the temperature remains constant with altitude.

2) The atmosphere acts as a grey absorber in the infrared region of the spectrum.

With these assumptions, the atmospheric temperature structure can be written as

$$T/T_g = (\tau/\tau_g)^{0.25} \tag{2.1}$$

where T is temperature, τ is infrared opacity increasing downward from the top of the atmosphere, and the subscript g refers to the planet's surface. The black-body flux B is equal to σT^4; therefore,

$$(B/B_g) = (\tau/\tau_g) \ . \tag{2.2}$$

The outgoing flux of radiation at the top of the atmosphere can now be written as

$$F(o) = B_g \, 2E_3(\tau_g) + (2B_g/\tau_g)\int_{\tau_t}^{\tau_g} \tau \, E_2(\tau)\,d\tau + (2B_g\tau_t/\tau_g)\int_o^{\tau} E_2(\tau)\,d\tau. \tag{2.3}$$

Upon integration, this equation can be written as

$$F(o) = B_g \left\{ 2E_3(\tau_g) + (2/3\tau_g)[\tau_t \, 2E_3(\tau_t) + e^{-\tau_t} - \tau_g \, 2E_3(\tau_g) - e^{-\tau_g}] \right.$$
$$\left. + (\tau_t/\tau_g)[1 - 2E_3(\tau_t)] \right\} \ . \tag{2.4}$$

If B_g, which depends solely on surface temperature, and τ_g and τ_t are known, the outgoing radiation can be computed from (2.4). It is assumed that τ_g and τ_t do not vary with latitude. The values of τ_g and τ_t to be used in (2.4) can be determined from the requirement that the average incoming solar radiation must equal the average outgoing radiation and the assumption that the stratosphere is, on the average, in gross infrared radiative equilibrium. The requirement can be written as

$$\bar{I}_o(1 - \bar{A}) = \bar{F}(o) = \sigma \bar{T}_g^4 \Big\{ 2E_3(\tau_g) + (2/3\tau_g)[\tau_t 2E_3(\tau_t) + e^{-\tau_t} - \tau_g 2E_3(\tau_g) - e^{-\tau_g}] + (\tau_t/\tau_g)[1 - 2E_3(\tau_t)] \Big\} \tag{2.5}$$

where $\bar{I}_o$ is the average incoming solar radiation at the top of the Martian atmosphere, $\bar{A}$ is the average Martian albedo, σ is the Stefan-Boltzmann constant, and $\bar{T}_g$ is the average surface temperature. The assumption can be written as

$$\bar{F}(o) = \bar{F}(\tau_t) \tag{2.6}$$

where $\bar{F}(o)$ is the average outgoing infrared radiation flux, and $\bar{F}(\tau_t)$ is the average infrared flux at the tropopause. For the present model, this requires that τ_g and τ_t be related through the following equation:

$$2E_3(\tau_g - \tau_t) + (2/\tau_g)\int_{\tau_t}^{\tau_g} \tau\, E_2(\tau - \tau_t)\,d\tau - 2(\tau_t/\tau_g)[1 - 2E_3(\tau_t)] = 2E_3(\tau_g) + (2/\tau_g)\int_{\tau_t}^{\tau_g} \tau\, E_2(\tau)\,d\tau \ . \tag{2.7}$$

The net incoming solar radiation can be written in terms of an effective black-body flux and temperature.

$$\bar{I}_o(1 - \bar{A}) = \bar{B}_e = \sigma \bar{T}_e^4 \quad . \tag{2.8}$$

Given the ratio of $\bar{T}_g$, the observed average surface temperature, to $\bar{T}_e$, the effective temperature the surface would have in the absence of an atmosphere, it is possible to determine τ_g and τ_t from Equations (2.5) and (2.7). In Section 3.1.5, we perform the reverse computation; that is, given τ_g, we compute (T_g/T_e) and τ_t.

The average incoming solar radiation is 0.215 cal $cm^{-2}min^{-1}$; the average albedo, from the values in Table 2.2, is 0.18. Consequently, the value of $\bar{T}_e$, based upon this new average albedo, is 216°K. The average surface temperature, from the values in Table 2.2, is 233°K, so that the ratio (T_g/T_e) is equal to 1.08. With $T_g/T_e = 1.08$, we find, from Table 3.4 of Section 3.1.5, that $\tau_g = 0.5$ and $\tau_t = 0.21$. Substituting these values into Equation (2.4), we find that

$$F(o) = .743\ B_g = .743\ \sigma\ T_g^4 \tag{2.9}$$

or, with $\sigma = 8.13 \times 10^{-11}$ cal cm^{-2} deg^{-4} min^{-1},

$$F(o) = 6.04 \times 10^{-11}\ T_g^4. \tag{2.10}$$

2.3.3 Results. Using Equation (2.10) and the surface temperatures listed in Table 2.2, we have computed the outgoing radiation flux as a function of latitude; these values are tabulated in the last column of Table 2.2. In Figure 2.2

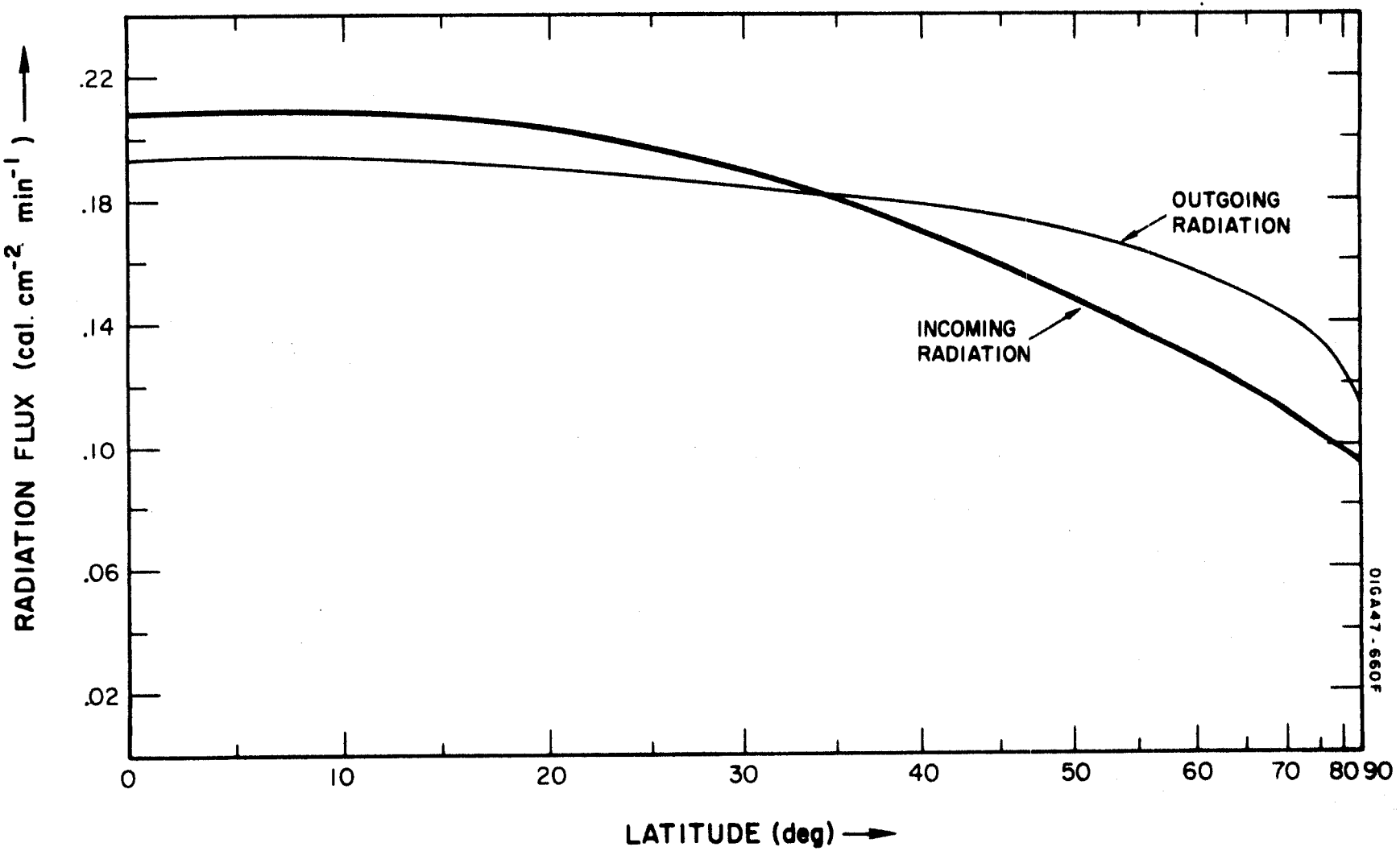

Figure 2.2. Annual radiation budget for planet Mars.

are plotted the variation with latitude of the net incoming solar radiation, $I_o(1 - A)$, and the outgoing radiation, F(o); the latitude scale is a cosine scale, so that length is proportional to the area of a latitude belt. These curves represent the annual radiation budget of the planet Mars. It can be noted, from Figure 2.2, that below latitude 35^o there is a surplus of energy, and above 35^o there is a deficit of energy. These curves are quite similar to those computed for the Earth (See, for example, London, 1957); for the Earth, the cross-over point is at about 40^o latitude. Since the temperature does not rise from year to year at equatorial regions, nor fall at polar regions, the excess heat energy in equatorial regions must be transported to higher latitudes. The average rate of transport across a fictitious wall at the cross-over latitude can be determined from the area between the net incoming radiation curve and the outgoing radiation curve, below the cross-over latitude. This turns out to be about 0.5×10^{16} cal min^{-1}; for the Earth, the corresponding figure is about 5×10^{16} cal min^{-1} (after London, 1957). The Martian value is an order of magnitude less than the value for the Earth, and there are probably several reasons for this. The primary reason is probably the difference in surface area between the two planets; the amount of heat energy to be transported past the cross-over latitude depends upon the surface area of the planet below the cross-over latitude- and Mars' surface area is a factor of 4 less than the Earth's surface area. Another reason is probably the difference between Earth and Mars in the dependence of outgoing radiation with latitude. On Mars, the variation with latitude of the outgoing radiation depends essentially

on the variation with latitude of the surface temperature; on Earth the latitudinal variation of outgoing radiation depends not only on the surface temperature variation but also on the water vapor variation with latitude. The latitudinal variation of water vapor in the Earth's atmosphere causes the latitudinal variation of outgoing radiation to be smaller than it would otherwise be. Hence, relatively larger differences between incoming and outgoing radiation occur, resulting in a larger value for the amount of excess heat energy.

With this information on the annual radiation budget, it is possible for dynamic meteorologists to infer the characteristics of the general circulation of a planet (See, for example, Mintz, 1961). Besides the annual radiation budget, it is desirable to have seasonal radiation budgets; further research in this area should be directed toward obtaining estimates of the seasonal budgets.

2.4 SUMMARY AND RECOMMENDATIONS

Emphasis was placed on three topics bearing on the meteorology of Mars -- (1) tides in the atmosphere of Mars, (2) construction of thermodynamic diagrams for the Martian atmosphere, and (3) the radiation budget of the Martian atmosphere.

The subject of tides in the Martian atmosphere was investigated with the aid of the standard tidal theory that has been developed for the earth's atmosphere. One of the possibilities in tidal oscillations is the presence of resonance magnification in a particular atmosphere. It occurs when an atmosphere has a free period close to that of the forcing function; in such a case any tidal oscillations would be amplified. Examination of this problem for Mars indicates that no resonance magnification is to be expected. The possibility that tidal oscillations might arise from the large diurnal temperature variations at the surface was considered; it appears highly improbable that the amplitude of the resulting diurnal surface-pressure oscillation (relative to total surface pressure) exceeds the amplitude of the Earth's semi-diurnal oscillation. Hence, tidal oscillations arising from this cause are not likely to play any significant role in the Martian general circulation. Tidal oscillations might also arise from diurnal or semi-diurnal temperature oscillations caused by periodic radiative processes occurring through deep layers of the Martian atmosphere. Present indications are that these oscillations are probably too small to excite significant tidal motions. Thus, this study concludes that in the light of present knowledge of the

Martian atmosphere, there is no reason to expect that tidal motions play an important role in the meteorology of Mars. If the Martian atmosphere should contain ozone in amounts greater than now suspected (or any other gas that absorbs significant amounts of solar radiation), then it is suggested that this conclusion be re-examined.

A preliminary thermodynamic diagram for use in analyzing thermodynamic processes in the Martian atmosphere has been constructed. The diagram is based upon a model Martian atmosphere, consisting of 83% nitrogen, 11% carbon dioxide, and 6% argon, with a surface pressure of 25 mb. Lines on the diagram include: pressures, dry adiabats, temperatures, saturation adiabats, and saturation specific humidities. Future research should be directed toward obtaining better estimates of surface pressure and atmospheric composition so that a final diagram can be prepared.

An estimate of the annual radiation budget for Mars — the average variation with latitude of net incoming solar radiation and outgoing infrared radiation — has been obtained. Net incoming solar radiation values are based upon the computations of Milankovitch (1920) and the planetary albedos estimated by Sagan (1964). Outgoing radiation values are a function only of the surface temperature, in the two-layer, grey-atmosphere model assumed for these calculations. The results indicate that between the equator and 35^{o} latitude there is a surplus of radiational energy, and above 35^{o} latitude there is a deficit. An average of 0.5×10^{16} cal min^{-1} must be transported across the 35^{o} latitude circle to maintain an annual balance; this is an order of magnitude less than the required

transport on the Earth. Further research should be directed toward obtaining estimates of the seasonal radiation budgets and utilizing these budgets in studies of the general circulation of the Martian atmosphere.

SECTION 3

METEOROLOGY OF VENUS

3.1 GREENHOUSE MODELS

3.1.1 Introduction. One of the most surprising results in the field of observational astronomy has been the recent finding that the surface temperature of Venus is remarkably high — about 600°- 700°K. The indications of high surface temperature are based upon observations from the earth of the planet's emission of microwave radiation (see Roberts [1963] for a summary of these observations); these indications have recently been confirmed by the microwave radiometer measurements made by the Mariner spacecraft on its Venus flyby (Barath et al., 1963). These temperatures are considered remarkable because they are two to three times the temperature expected on Venus on the basis of its distance from the sun and its planetary albedo. This discrepancy between the expected and the observed has stimulated a good deal of research to explain the cause of the high temperatures.

One means by which the surface temperature of a planet can be kept high is the greenhouse mechanism. For this mechanism to be effective the atmosphere must be relatively transparent to incoming solar radiation and

relatively opaque to outgoing infrared radiation. In previous models of the greenhouse mechanism the effect of the extensive cloud cover of Venus on the transfer of infrared radiation has not been directly considered. In the present studies the effect of a cloud cover, opaque to infrared radiation, on greenhouse models of the atmosphere of Venus are investigated.

A large greenhouse effect as an explanation of the high surface temperature of Venus was suggested by Sagan (1960). He used the following equation for the balance of incoming solar and outgoing infrared radiation at the top of the Venus atmosphere:

$$\sigma T_e^4 = \sigma T_a^4 + t\sigma T_g^4$$

where σ is the Stefan-Boltzmann constant, T_e is the effective temperature of the incoming solar radiation (allowing for albedo losses), T_a is the effective radiating temperature of the atmosphere, T_g is the planetary surface temperature, and t is the transmissivity of the atmosphere for infrared radiation. The left side of the equation represents the incoming solar radiation; the right side, the outgoing infrared radiation. With this equation Sagan was able to compute the atmospheric infrared transmissivity required to maintain a $600^{\circ}K$ surface temperature. Assuming $T_a = 234^{\circ}K$, he obtained a required transmissivity of about 0.9 per cent for the case of $T_e = 254^{\circ}K$ (corresponding to an albedo of 0.64), and 0.2 per cent for the case of $T_e = 240^{\circ}K$ (corresponding to an albedo of 0.71). Making use of laboratory emissivity measurements of carbon dioxide and

water vapor, he found that 18 km STP of carbon dioxide together with 9 g cm^{-2} of water vapor could produce the required transmissivities. Since these amounts of gases are not incompatible with present knowledge of the Venus atmosphere, a strong greenhouse effect appears possible.

However, another theoretical attack on the problem, by Jastrow and Rasool (1963), with a different approach led to a different conclusion. Making use of the Eddington approximation to compute the radiative equilibrium temperature distribution in the atmosphere of Venus, they found that the required infrared transmissivities for a 600°K temperature were so small as to be incompatible with present knowledge of the composition of the Venus atmosphere. For a gray atmosphere in radiative equilibrium the Eddington approximation leads to the following formula for surface temperature:

$$T_g = T_e(1 + 0.75\tau_g)^{1/4}$$

where τ_g is the atmospheric opacity in the infrared. For a T_e value of 254°K the required opacity is about 40, and for a T_e value of 240°K the required opacity is about 50. These opacities correspond to transmissivities less than 10^{-22}, or many orders of magnitude less than those required in Sagan's model. The basic cause of the difference between the two models is Sagan's choice of 234°K for T_a; the required transmissivity depends critically upon the value of T_a, which is really unknown and must be assumed.

The effect of cloud cover on the infrared radiation leaving the planet has not been specifically included in the two previous approaches. The amount of cloud cover in the Venus atmosphere is large, and if the cloud cover acts as a blackbody for infrared radiation, as the water clouds of the earth's atmosphere do, it should enhance the greenhouse effect.

In our research, we have developed two greenhouse models—a one layer model and a two layer model—both of which include the effect of cloudiness. Descriptions of these two models and the results obtained are presented in the following sections.

3.1.2 One-layer greenhouse model. NOTE: The subject matter of this section has been treated in detail in the following two references—the first a technical report under the present contract, the other a paper in the scientific literature, based upon the technical report.

Ohring, G. and Mariano, J., 1963: "The effect of cloudiness on a greenhouse model of the Venus atmosphere," GCA Technical Report No. 63-17-N, Contract NASw-704, p. 28.

Ohring, G. and Mariano, J., 1964: "The effect of cloudiness on a greenhouse model of the Venus atmosphere," Journal of Geophysical Research, 69, 165-175.

We present here a summary of the reported work; for a complete discussion, consult either of the above references.

In the one-layer greenhouse model, the following assumptions are made:

(1) There is a balance between net incoming solar radiation and outgoing infrared radiation at the top of the atmosphere.

(2) The atmosphere consists of one layer, which is characterized by a linear variation of temperature with altitude.

(3) Venus has a grey atmosphere with constant absorption coefficient for infrared radiation.

(4) The cloud cover is opaque to infrared radiation and is not 100% complete.

For this model, the outgoing flux of infrared radiation at the top of the atmosphere can be written as

$$F(0) = (1-n)\, B_g \left[2\, E_3(\tau_g) + 2\, \tau_g^{-4k} \int_0^{\tau_g} \tau^{4k}\, E_2\,(\tau)\, d\tau \right] + \tag{3.1}$$

$$+ n\, B_g \left[2\, E_3\,(p\tau_g)\, p^{4k} + 2\tau_g^{-4k} \int_0^{p\tau_g} \tau^{4k}\, E_2\,(\tau)\, d\tau \right]$$

where n is the fraction of the sky covered by clouds; τ is the infrared opacity of the atmospheric gases, increasing from zero at the top of the atmosphere to τ_g at the surface; the E's are exponential integrals; k is the constant in the relationship between temperature, T, and pressure, p, in an atmosphere with linear variation of temperature with altitude, $T_a/T_g = (p_a/p_g)^k$, where the subscripts a and g refer to the

atmosphere and surface, respectively; p is the ratio of the infrared opacity of the atmosphere above the cloud-top, τ_c, to the infrared opacity of the entire atmosphere, τ_g (or, since the opacity is proportional to the pressure in this grey atmosphere, p is the ratio of cloud-top pressure to surface pressure); and B is the blackbody flux, σT^4, which varies with opacity according to $B/B_g = (\tau/\tau_g)^{4k}$.

With the requirement that the outgoing radiation must balance the net incoming solar radiation, or $F(0) = \sigma T_e^4$, where T_e is the effective temperature of the net incoming solar radiation, one can obtain an expression relating the magnitude of the greenhouse effect to the amount of cloudiness, height of cloud-top (as represented by p), and the atmospheric infrared opacity

$$\left(\frac{T_e}{T_g}\right)^4 = (1-n)\left[2\,E_3(\tau_g) + 2\tau_g^{-4k}\int_o^{\tau_g}\tau^{4k}\,E_2(\tau)\,d\tau\right] + n\left[2\,E_3(p\tau_g)\,p^{4k} + 2\tau_g^{-4k}\int_o^{p\tau_g}\tau^{4k}\,E_2(\tau)\,d\tau\right] \qquad (3.2)$$

The ratio (T_g/T_e) is the ratio of the greenhouse surface temperature to the surface temperature that Venus would have without an atmosphere; this ratio represents the magnitude of the greenhouse effect.

For values of 4k equal to integers, the integrals in Equation (3.2) can be evaluated analytically. Of physical interest is the case 4k = 1, k = 0.25, which corresponds to an atmosphere with a temperature lapse-rate of 0.9 of the adiabatic lapse-rate. In this case, Equation (3.2) becomes

$$\left(\frac{T_e}{T_g}\right)^4 = \frac{1-n}{3}\left\{2\tau_g^{-1}[1 - \exp(-\tau_g)] + 2E_3(\tau_g)\right\}$$

$$= \frac{np}{3}\left\{2(p\tau_g)^{-1}[1 - \exp(-p\tau_g)] + 2E_3(p\tau_g)\right\} \qquad (3.3)$$

For values of 4k not equal to integers, the integrals in Equation (3.2) can be evaluated numerically. Of particular interest is the adiabatic case k = 0.286, which maximizes the greenhouse surface temperature.

Computations of the magnitude of the greenhouse effect have been performed with both the adiabatic lapse-rate and 0.9 the adiabatic lapse-rate, for a range of values of the parameters τ_g, n, and p. The results of these computations are presented in Tables 3.1a, 3.1b, 3.1c, and 3.1d. It should be noted that the values for p = 1 represent conditions for a cloud-top located at the surface, or, more importantly, the case of no clouds at all. The importance of cloudiness can be ascertained by comparing the values for p = 1 to the other computed values.

With the use of these tables and graphs based upon them, one can obtain estimates of atmospheric infrared opacity required to maintain the observed greenhouse effect on Venus. The observed surface temperature is about 600°K to 700°K. With an albedo of 0.73 (Sinton, 1962), T_e is 237°K. The Mariner infrared observations, which detected no breaks in the cloud layer (Chase, et al., 1963), the telescopic

Table 3.1a

Summary of computations of magnitude of greenhouse effect, T_g/T_e, for one-layer model with 80% cloudiness.

τ_g	T_g/T_e (k = .286)	T_g/T_e (k = .25)	T_g/T_e (k = .286)	T_g/T_e (k = .25)
	p = .002		p = .05	
1	1.804	1.776	1.705	1.644
2	2.053	1.994	1.885	1.787
3	2.262	2.171	2.020	1.890
5	2.591	2.441	2.206	2.031
10	3.130	2.862	2.472	2.232
20	3.751	3.322	2.786	2.480
30	4.142	3.599	3.023	2.667
	p = .01		p = .10	
1	1.788	1.749	1.618	1.553
2	2.023	1.948	1.764	1.669
3	2.215	2.102	1.872	1.755
5	2.504	2.325	2.028	1.878
10	2.933	2.635	2.285	2.085
20	3.361	2.949	2.646	2.370
30	3.604	3.116	2.930	2.599
	p = .02		p = .50	
1	1.767	1.719	1.319	1.284
2	1.985	1.898	1.451	1.401
3	2.158	2.033	1.567	1.502
5	2.407	2.140	1.764	1.669
10	2.756	2.472	2.128	1.969
20	3.099	2.722	2.593	2.344
30	3.311	2.881	2.912	2.591
	p = 1			
1	1.209	1.192		
2	1.377	1.342		
3	1.519	1.465		
5	1.746	1.656		
10	2.127	1.968		
20	2.593	2.340		
30	2.912	2.590		

Table 3.1b

Summary of computations of magnitude of greenhouse effect, T_g/T_e, for one-layer model with 90% cloudiness.

τ_g	T_g/T_e (k = .286)	T_g/T_e (k = .25)	T_g/T_e (k = .286)	T_g/T_e (k = .25)
	p = .002		p = .05	
1	2.141	2.102	1.913	1.814
2	2.433	2.353	2.071	1.931
3	2.676	2.554	2.182	2.012
5	3.054	2.854	2.329	2.119
10	3.654	3.300	2.541	2.281
20	4.305	3.749	2.816	2.500
30	4.681	3.994	3.038	2.677
	p = .01		p = .10	
1	2.100	2.035	1.755	1.662
2	2.358	2.241	1.872	1.751
3	2.560	2.394	1.958	1.818
5	2.849	2.600	2.084	1.919
10	3.238	2.863	2.310	2.104
20	3.585	3.101	2.653	2.377
30	3.774	3.226	2.933	2.599
	p = .02		p = .50	
1	2.048	1.965	1.337	1.298
2	2.270	2.135	1.462	1.409
3	2.435	2.254	1.574	1.507
5	2.657	2.409	1.767	1.671
10	2.940	2.604	2.128	1.969
20	3.209	2.798	2.593	2.344
30	3.384	2.932	2.912	2.591
	p = 1			
1	1.209	1.192		
2	1.377	1.342		
3	1.519	1.465		
5	1.746	1.656		
10	2.127	1.968		
20	5.593	2.340		
30	2.912	2.590		

Table 3.1c

Summary of computations of magnitude of greenhouse effect, T_g/T_e, for one-layer model with 95% cloudiness.

τ_g	T_g/T_e (k = .286)	T_g/T_e (k = .25)	T_g/T_e (k = .286)	T_g/T_e (k = .25)
	p = .002		p = .05	
1	2.536	2.472	2.086	1.944
2	2.873	2.757	2.210	1.958
3	3.150	2.977	2.294	2.090
5	3.571	3.290	2.405	2.172
10	4.203	3.725	2.579	2.308
20	4.821	4.114	2.831	2.511
30	5.146	4.306	3.016	2.683
	p = .01		p = .10	
1	2.439	2.327	1.850	1.731
2	2.704	2.521	1.941	1.805
3	2.900	2.656	2.009	1.854
5	3.159	2.825	2.115	1.941
10	3.472	3.028	2.322	2.113
20	3.730	3.193	2.657	2.377
30	3.876	3.297	2.934	2.608
	p = .02		p = .50	
1	2.328	2.192	1.346	1.306
2	2.533	2.334	1.468	1.414
3	2.673	2.427	1.577	1.509
5	2.848	2.542	1.768	1.672
10	3.059	2.684	2.128	1.969
20	3.272	2.840	2.593	2.344
30	3.424	2.958	2.912	2.591
	p = 1			
1	1.209	1.192		
2	1.377	1.342		
3	1.519	1.465		
5	1.746	1.656		
10	2.127	1.968		
20	2.593	2.340		
30	2.912	2.590		

Table 3.1d

Summary of computations of magnitude of greenhouse effect, T_g/T_e, for one-layer model with 99% cloudiness.

τ_g	T_g/T_e (k = .286)	T_g/T_e (k = .25)	T_g/T_e (k = .286)	T_g/T_e (k = .25)
	p = .002		p = .05	
1	3.674	3.468	2.308	2.093
2	4.086	3.751	2.366	2.134
3	4.395	3.942	2.408	2.166
5	4.804	4.175	2.476	2.223
10	5.285	4.424	2.612	2.330
20	5.626	4.597	2.845	2.520
30	5.772	4.671	3.053	2.687
	p = .01		p = .10	
1	3.184	2.870	1.950	1.800
2	3.367	2.973	2.000	1.845
3	3.479	3.035	2.055	1.886
5	3.604	3.104	2.142	1.959
10	3.740	3.188	2.333	2.118
20	3.872	3.280	2.660	2.380
30	3.969	3.353	2.935	2.604
	p = .02		p = .50	
1	2.824	2.531	1.354	1.312
2	2.929	2.592	1.472	1.417
3	2.992	2.631	1.580	1.511
5	3.068	2.680	1.769	1.672
10	3.177	2.758	2.128	1.969
20	3.328	2.876	2.593	2.340
30	3.459	2.980	2.912	2.590
	p = 1			
1	1.209	1.192		
2	1.377	1.342		
3	1.519	1.465		
5	1.746	1.656		
10	2.127	1.968		
20	2.593	2.340		
30	2.912	2.590		

observations, and the large visual albedo, all suggest a very extensive cloud cover. Therefore, we can use the computations for 99% cloudiness. The Mariner infrared observations also suggest a cloud-top temperature of 240°K, from which we can determine the appropriate value of p. In Table 3.2 are shown the infrared opacities required to maintain the observed surface temperatures on Venus. To maintain a surface temperature of 700°K, which is probably closer to the true average, atmospheric opacities of about six or seven are required, corresponding to transmissivities of 0.06% and 0.02%, respectively. To maintain a 600°K surface temperature, atmospheric opacities of two or three are required. Infrared opacities of six or seven are relatively high

TABLE 3.2

INFRARED OPACITIES REQUIRED TO MAINTAIN OBSERVED SURFACE TEMPERATURE ON VENUS

n	T_g (°K)	T_g/T_e	T_{cloud} (°K)	k	p	Required Opacity, τ_g
0.99	700	2.95	240	0.286	0.024	6
0.99	700	2.95	240	0.25	0.014	7
0.99	600	2.5	240	0.286	0.041	2.5
0.99	600	2.5	240	0.25	0.026	3

and suggest that the Venus atmosphere must contain large amounts of water vapor, or other infrared absorbing constituents, besides carbon

dioxide. Infrared opacities of two or three are relatively low and could possibly be produced by carbon dioxide alone. The required infrared opacities depend initially upon the height and temperature of the cloud top. For example, with a cloud-top temperature of 220°K, an infrared opacity of only 1.5 is required to maintain a 700°K surface temperature. Until these parameters are known more accurately, definitive calculations cannot be performed.

The one-layer greenhouse model illustrates the importance of the amount and height of clouds for the maintainence of high surface temperatures. The presence of a cloud that is opaque to infrared radiation enhances the greenhouse effect, since, with the temperature decreasing with height, the cloud will absorb the high-temperature surface radiation and reradiate to space at lower temperatures. A number of assumptions are made in the development of the model; to the extent that these assumptions are invalid, the final results may be in question. The assumption of a grey atmosphere is incorrect; just how much this assumption influences the final results is unknown. It is implicitly assumed that the absorbing gases are uniformly mixed with height; departures from constant mixing ratios would affect the final results. The clouds are assumed to be completely opaque to infrared radiation; any departures from complete opaqueness would certainly influence the results presented here. The assumption of complete opaqueness for the clouds is probably the cause of questionable internal side-effects; these side-effects are discussed in Ohring and Mariano (1964). Other uncertainties are introduced by the assumption

of a one-layer model with temperature decreasing with altitude at a constant rate to the top of the atmosphere, and the implicit assumption of a surface infrared emissivity of unity. And last, but perhaps not least, it is implicitly assumed that there is a negligible amount of absorption of solar radiation in the atmosphere; this assumption, which has been made in previous Venus greenhouse models, is certainly questionable, and its effect should be evaluated in more realistic models.

Some of these uncertainties are discussed in the following sections.

3.1.3 Effect of Emissivity of Venus' Surface. In the greenhouse calculations it has been assumed that the emissivity of the surface of Venus is unity. There are indications, at least in the microwave portion of the spectrum, that the emissivity is less than unity. The radar returns from Venus indicate emissivities of about 0.9 (Victor, Stevens, and Golumb, 1961). If this is true for the entire infrared emission spectrum, then one should consider this in the calculations of the greenhouse effect. We have performed calculations with a surface emissivity of 0.9 in order to examine the change in greenhouse effect that would be produced.

If the infrared emissivity of the Venus surface is 0.9, the outgoing radiation at the top of the atmosphere in the clear part of the sky can be written as

$$F(o)_{clear} = \left[2E_3(\tau_g)\ 0.9\ B_g + 2\ B_g \tau_g^{-4k} \int_o^{\tau_g} \tau^{4k}\ E_2(\tau) d\tau\right] (1-n) \quad (3.4)$$

With a value of k = 0.25, corresponding to a temperature lapse rate of about 0.9 of the adiabatic lapse rate, and with n amount of clouds, the greenhouse effect becomes

$$\left(\frac{T_e}{T_g}\right)^4 = \frac{(1 - n)}{3} \left[\frac{2}{\tau_g} (1 - \exp [-\tau_g]) + (0.7)\ 2E_3(\tau_g)\right] + \frac{np}{3} \left[\frac{2}{p\tau_g} (1 - \exp [-p\tau_g]) + 2E_3(p\tau_g)\right] \quad (3.5)$$

This formula is similar to that derived for an emissivity of unity, Equation (3.3), except that with an emissivity value of 0.9 the factor 0.7 is introduced as a multiplier of $2E_3(\tau_g)$ on the right side of the equation.

For the range of opacities and cloud amounts thought to prevail on Venus, the greenhouse effect is not substantially changed by introducing a surface emissivity of 0.9. One would expect the largest changes for small cloud amounts and atmospheric infrared opacities, and high cloud heights; this is seen to be the case in Figures 3.1 and 3.2, where the greenhouse effect is shown for cloud amounts n = 0.8 and n = 0.99, emissivity, e, equal to 0.9 and 1.0, and ratio of cloud top pressure to surface pressure, p, equal to 0.002 and 0.5. But even these changes are small enough to be neglected. Thus, we may conclude that the use of a surface emissivity of 0.9 rather than 1.0 would not substantially alter the greenhouse effect on Venus.

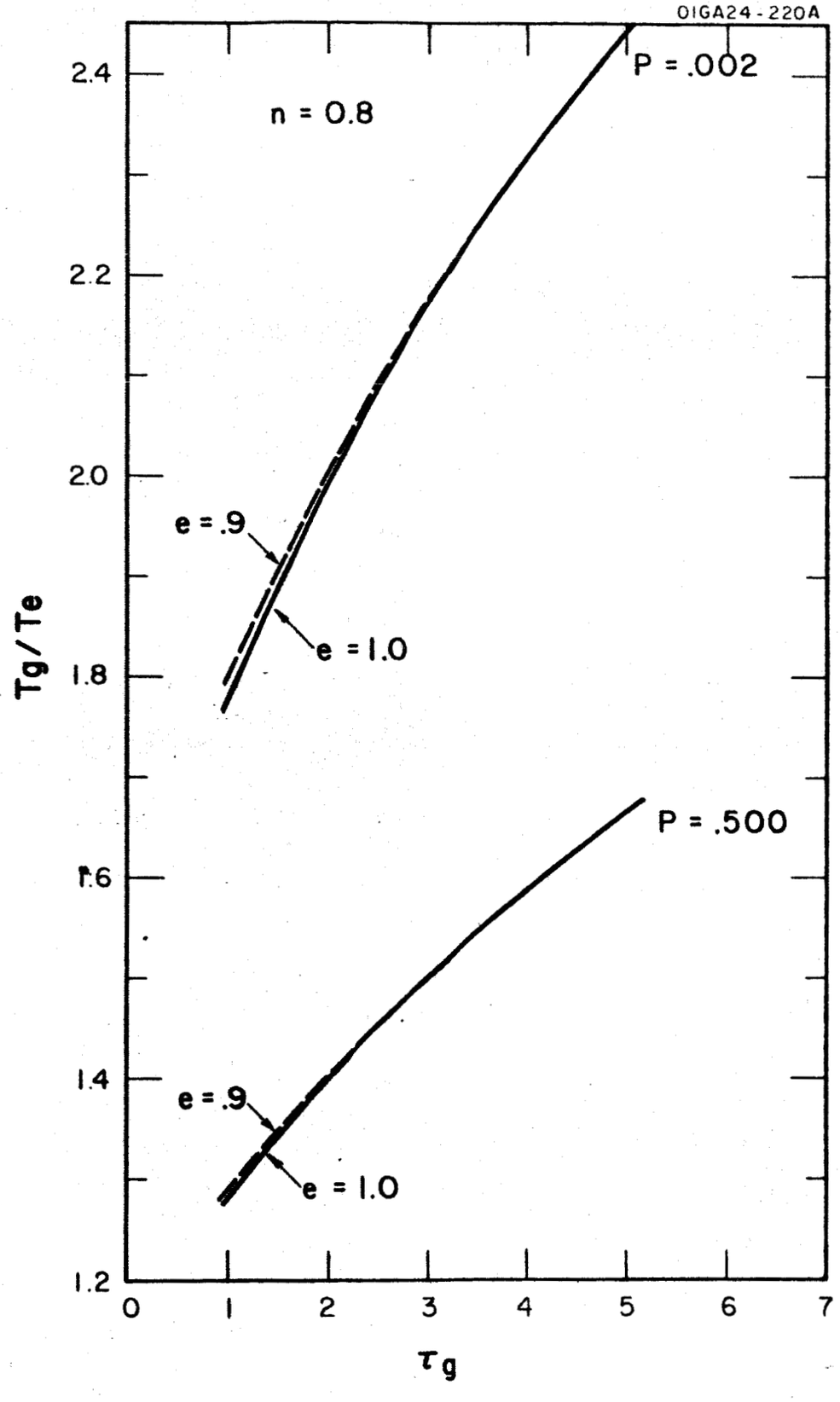

Figure 3.1. **Magnitude of the greenhouse effect on Venus for surface emissivities of 0.9 and 1.0 for 80% cloud cover.**

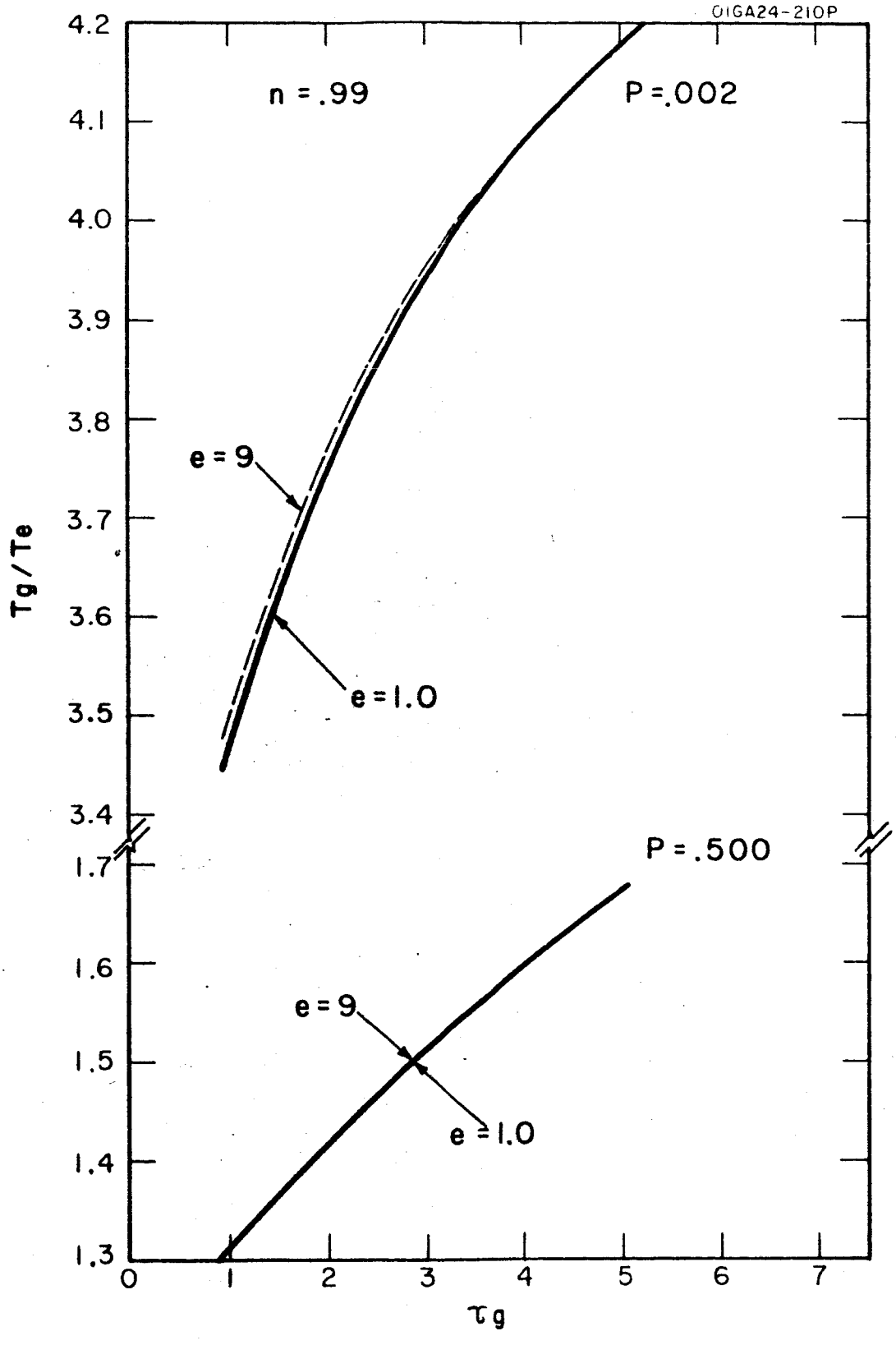

Figure 3.2. **Magnitude of the greenhouse effect on Venus for surface emissivities of 0.9 and 1.0 for 99% cloud cover.**

3.1.4 Two-layer Greenhouse Model. One of the unrealistic assumptions in the one-layer greenhouse model is the assumption of constant lapse-rate, which implies that the temperature decreases to zero at the top of the atmosphere. This is certainly not the case in the earth's atmosphere and is probably not the case in the Venus atmosphere. A simplified model of the earth's atmosphere would consist of two layers: a troposphere in which the temperature lapse-rate is constant and a stratosphere in which the temperature lapse-rate is zero. We can assume that the Venus atmosphere has a similar structure. If we further assume that the stratospheric layer is in radiative equilibrium, we can actually compute, as will be shown later, the height of the tropospause - the level at which the temperature starts to remain constant with altitude. The following sketch illustrates the assumed model atmosphere.

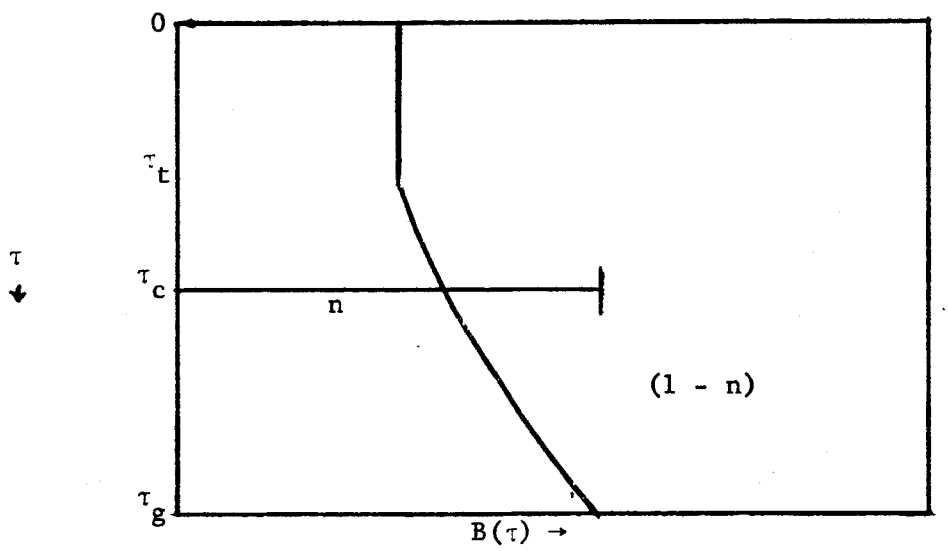

In the troposphere, temperature is related to pressure by

$$\frac{T_a}{T_g} = \left(\frac{p_a}{p_g}\right)^k \qquad (3.6)$$

For a grey atmosphere with constant mixing ratio of absorbing gas, the blackbody flux, $B = \sigma T^4$, in the troposphere is then related to infrared opacity, τ, by

$$\frac{B(\tau)}{B(\tau_g)} = \left(\frac{\tau}{\tau_g}\right)^{4k} \tag{3.7}$$

In the stratosphere, B is constant since the temperature is constant with altitude. The distribution of B as a function of τ is shown schematically in the sketch. The tropopause is located at the level τ_t and the cloud top is located at the level τ_c. The fraction of the sky covered by clouds is n, leaving a clear portion (1 - n).

Our goal is to compute the greenhouse effect, represented by the ratio T_g/T_e, where T_e is the effective temperature of incoming solar radiation and T_g is the surface temperature, and to compute the height of tropopause τ_t. Once these quantities are computed the entire atmospheric temperature structure is defined. These quantities can be computed on the basis of two equilibrium conditions:

(1) The incoming solar radiation balances the outgoing infrared radiation at the top of the atmosphere.

(2) The net flux of infrared radiation at the tropopause is equal to the outgoing infrared radiation at the top of the atmosphere. Since it is assumed that there is no absorption of solar radiation in

the stratosphere, this condition implies a gross radiative equilibrium for the stratospheric layer.

The upward flux of radiation at the tropopause in the clear part of the atmosphere can be written as

$$F\uparrow(\tau_t)_{clear} = (1 - n)[B_g\ 2E_3(\tau_g - \tau_t) + 2\int_{\tau_t}^{\tau_g} B(\tau)\ E_2(\tau - \tau_t)d\tau] \qquad (3.8)$$

where n is the fraction of cloudiness, B is the black-body flux, the E's are exponential integrals, and the subscript g refers to the planet's surface.

With the use of Equation (3.7), the clear-sky upward flux at the tropopause can be written as

$$F\uparrow(\tau_t)_{clear} = (1 - n)[B_g\ 2E_3(\tau_g - \tau_t) + \frac{2B_g}{\tau_g^{4k}}\int_{\tau_t}^{\tau_g} \tau^{4k}\ E_2(\tau - \tau_t)d\tau]. \qquad (3.9)$$

If τ_c/τ_g is represented by p, the expression for the upward flux of radiation at the tropopause in the cloudy part of the sky can be written as

$$F\uparrow(\tau_t)_{cloudy} = n[p^{4k}\ B_g\ 2E_3(p\tau_g - \tau_t) + \frac{2B_g}{\tau_g^{4k}}\int_{\tau_t}^{p\tau_g} \tau^{4k}\ E_2(\tau - \tau_t)\ d\tau]. \qquad (3.10)$$

The total upward flux at the tropopause is the sum of the contributions from clear and cloudy skies

$$F\uparrow(\tau_t) = F\uparrow(\tau_t)_{clear} + F\uparrow(\tau_t)_{cloudy} \quad . \tag{3.11}$$

The downward flux of radiation at the tropopause is

$$F\downarrow(\tau_t) = 2B(\tau_t) \int_0^{\tau_t} E_2(\tau)d\tau \quad . \tag{3.12}$$

The net flux of radiation at the tropopause is

$$F_{net}(\tau_t) = F\uparrow(\tau_t) - F\downarrow(\tau_t) \quad . \tag{3.13}$$

The expression for the outgoing flux at the top of the atmosphere is

$$F(o) = (1 - n)\left[B_g\ 2E_3(\tau_g) + \frac{2B_g}{\tau_g^{4k}} \int_{\tau_t}^{\tau_g} \tau^{4k}\ E_2(\tau)d\tau + 2B(\tau_t) \int_0^{\tau_t} E_2(\tau)d\tau\right] +$$

$$+ n\left[B_g p^{4k}\ 2E_3(p\tau_g) + \frac{2B_g}{\tau_g^{4k}} \int_{\tau_t}^{p\tau_g} \tau^{4k}\ E_2(\tau)d\tau + 2B(\tau_t) \int_0^{\tau_t} E_2(\tau)d\tau\right] . \tag{3.14}$$

The condition that the stratosphere be in radiative equilibrium can be expressed as

$$F(o) - F_{net}(\tau_t) = 0 \quad . \tag{3.15}$$

The condition that the incoming solar radiation balance the outgoing infrared radiation at the top of the atmosphere can be written as

$$F(o) = \sigma T_e^4 \qquad (3.16)$$

From the expanded form of Equation (3.15) one can obtain an equation that will allow computation of τ_t when τ_g, n, p, and k are given. Making use of the relation

$$B(\tau_t) = B_g\left(\frac{\tau_t}{\tau_g}\right)^{4k}$$

and

$$\int_o^{\tau_t} E_2(\tau)\, d\tau = \frac{[1 - 2E_3(\tau_t)]}{2} \quad ,$$

we can obtain the following equation from the expanded form of (3.15)

$$(1 - n)\left[2E_3(\tau_g - \tau_t) + \frac{2}{\tau_g^{4k}} \int_{\tau_t}^{\tau_g} \tau^{4k} E_2(\tau - \tau_t)d\tau\right] +$$

$$+ n\left[p^{4k}\, 2E_3(p\tau_g - \tau_t) + \frac{2}{\tau_g^{4k}} \int_{\tau_t}^{p\tau_g} \tau^{4k} E_2(\tau - \tau_t)d\tau\right] -$$

$$-2\left(\frac{\tau_t}{\tau_g}\right)^{4k}\left[1 - 2E_3(\tau_t)\right] = (1 - n)\left[2E_3(\tau_g) + \frac{2}{\tau_g^{4k}} \int_{\tau_t}^{\tau_g} \tau^{4k} E_2(\tau)d\tau\right] +$$

$$+ n\left[p^{4k} 2E_3(p\tau_g) + \frac{2}{\tau_g^{4k}} \int_{\tau_t}^{p\tau_g} \tau^{4k} E_2(\tau) d\tau \right] \qquad (3.17)$$

In principle, (3.17) can be solved for τ_t if the other variables are given; techniques for numerical solution are presented below.

Once τ_t is determined, it can be substituted into the expanded form of (3.16) to obtain the magnitude of the greenhouse effect from

$$\left(\frac{T_e}{T_g}\right)^4 = (1 - n)\left[2E_3(\tau_g) + \frac{2}{\tau_g^{4k}} \int_{\tau_t}^{\tau_g} \tau^{4k} E_2(\tau) d\tau\right] +$$

$$+ n\left[p^{4k} 2E_3(p\tau_g) + \frac{2}{\tau_g^{4k}} \int_{\tau_t}^{p\tau_g} \tau^{4k} E_2(\tau) d\tau\right] + \left(\frac{\tau_t}{\tau_g}\right)^{4k}\left[1 - 2E_3(\tau_t)\right] . \qquad (3.18)$$

Since the unknown variable, τ_t, appears in the limits of the integrals, an iterative technique had to be used to solve Equation (3.17). Because of the complexity of the problem and the relatively small storage capacity of the IBM 1620 computer, the following straightforward method was adopted: A trial value of τ_t is read into the program; the right and left hand sides of Equation (3.17) are computed, where τ_t equals the trial value; and the difference between right and left hand sides of Equation (3.17), $D(\tau_t)$, is printed along with the corresponding τ_t value. Thus at any time during the entire computation, one can observe the trend of $D(\tau_t)$ from the values of $D(\tau_t)$ and continually

improve his choice of trial values. There exist two solutions to Equation (3.17), the trivial solution, $\tau_t = 0$, $\left(D(o) = 0\right)$, and some value (say τ_t^*) between $\tau_t = 0$ and $\tau_t = \tau_g$, $\left(D(\tau_t^*) = 0\right)$. Hence, the curve of the function, $D(\tau_t)$, must cross the "τ" axis at τ_t^*, the non-trivial solution to Equation (3.17). As soon as a change in the sign of $D(\tau_t)$ occurs, one can either extrapolate the curve $D(\tau_t)$ to get τ_t^*, or read in a "finer" set of points in the neighborhood where $D(\tau_t)$ changes in sign, and thus narrow the range of τ_t values. By continuing this latter process, τ_t^* can be evaluated to four digit accuracy.

The bulk of the program was in evaluating the exponential integrals, $E_2(x)$ and $E_3(x)$, and the four integrals of Equation (3.17). $E_2(x)$ and $E_3(x)$ were evaluated by first reducing them to the first exponential integral, $E_1(x)$, by the relation (Chandrasekhar, 1960):

$$n\,E_{n+1}(x) = e^{-x} - x\,E_n(x) \qquad (n \geq 1)$$

and then evaluating $E_1(x)$ from the following approximation:

$$E_1(x) \approx -\gamma - \ell n\, x + \sum_{n=1}^{10} \frac{(-1)^{n-1} x^n}{n \cdot n!} \quad , \qquad \text{for } x \leq 1,$$

where $\gamma = 0.5772157$, and:

$$E_1(x) \approx \frac{e^{-x}}{x} \left\{ \frac{a_o + a_1 x + a_2 x^2 + a_3 x^3 + x^4}{b_o + b_1 x + b_2 x^2 + b_3 x^3 + x^4} \right\}$$

$a_o = .2677737$

$a_1 = 8.634761$

$a_2 = 18.05902$

$a_3 = 8.573329$

$b_o = 3.958497$

$b_1 = 21.09965$

$b_2 = 25.63296$

$b_3 = 9.573322$

for $x > 1$. (These equations are derived by Chandrasekhar (1960) and Hastings (1955) respectively). Since the four integrals of Equation (317) are of the same form, the problem of their solutions reduces to evaluating integrals of the form:

$$I(x) = \int_{a(x)}^{b(x)} \xi^{\alpha} E_2(c + \xi)\, d\xi$$

where α and c are constants. The approximation to this integral is derived from Weddle's rule, which is (Kunz, 1957):

$$\int_a^b f(x)\, dx = \frac{3}{10} h\, (f_o + 5f_1 + f_2 + 6f_3 + f_4 + 5f_5 + f_6) ,$$

where the interval of integration, b - a, is divided into six equal sub-intervals of length,

$$h = \frac{b - a}{6}$$

and

$$f_o = f\ (a)$$

$$f_1 = f\ (a + h)$$

$$f_2 = f\ (a + 2h)$$

.

.

.

$$f_6 = f\ (a + 6h) = f\ (b)$$

This equation can be slightly generalized to include any integral multiple of six (say N, where N = 6I, I = 1, 2, 3, ...) points. This is done by dividing the interval (b - a) by N and using Weddle's rule for each of the following right hand terms:

$$\int_a^b f(x)\,dx = \int_a^{a+\frac{(b-a)}{N}} f(x)\,dx + \int_{a+\frac{(b-a)}{N}}^{a+\frac{2(b-a)}{N}} f(x)\,dx + \ldots + \int_{a+(N-1)\frac{(b-a)}{N}}^{b} f(x)\,dx \qquad (3.19)$$

Let

$$f_k = f\left[a + \frac{k(b - a)}{N}\right] \qquad (k = 1, 2, \ldots., N)$$

and Equation (3.19) reduces to:

$$\int_a^b f(x)\,dx = \frac{3}{10}\,\frac{(b-a)}{N}\left[(f_o + f_6 + f_{12} + \ldots + f_N) + \right.$$

$$+ (f_2 + f_4 + f_6 + \ldots + f_{N-2}) + (f_3 + f_9 + f_{15} + \ldots + f_{N-3}) +$$

$$\left. + 5\,(f_1 + f_3 + f_5 + \ldots\, f_{N-1})\right] \quad . \tag{3.20}$$

In the problem at hand,

$$F(x) = x^{\alpha}\, E_2(c + x) \ .$$

and I is made equal to the largest integer in the length, (b - a), thus making the number of points, N = 6I, proportional to the length to integration.

Once the value of τ_t satisfying Equation (3.17) is found, T_g/T_e is readily calculated from Equation (3.18), for the integrals and exponential integrals of Equation (3.18) are identical to those of Equation (3.17).

The exponential integrals, $E_2(x)$ and $E_3(x)$ of Equations (3.18) and (3.19) are accurate to seven places, and the integrals of Equations (3.18) and (3.19) are accurate to four places, and thus $D(\tau_t)$ is accurate to four digits. Since numerical values of τ_t and T_g/T_e to only three digit accuracy were desired, the errors propagated in the computations lie outside the scope of interest. However, accuracy up to seven places can easily be achieved [by increasing the number of points in the integral approximation Equation (3.20)] through minor program changes.

Computations were performed with the two-layer model for 99% cloudiness, and for several values of τ_g, k, and p that might be applicable to Venus. The results of these computations are summarized in Table 3.3. In the first set of computations in this table, the cloud-top temperature is assumed to be 240°K and k is equal to either 0.286 or 0.25. From this set it can be seen that a surface temperature of ~ 600°K requires an infrared opacity of about 3, and a surface temperature of about 700°K requires an infrared opacity of about 6 or 7. These results are in close agreement with the results of the one-layer model computations. The reason for this agreement is the relatively thin stratosphere (in terms of mass), which does not greatly change the outgoing radiation from that computed for the one-layer model. The ratio τ_t/τ_g, which is equivalent to ratio of tropopause pressure to surface pressure, is seen to be of the order of 1 or 2% in this set of computations. The second set of Venus computations is based upon an atmospheric model suggested by Kaplan (1962). Kaplan's values of k and p are used for these computations. For this model atmosphere an infrared opacity of about 7 is required to produce a surface temperature of 700°K. The ratio τ_t/τ_g for this set is of the order 2×10^{-4}.

A comparison of the one-layer and two-layer greenhouse models for the case of no clouds and a lapse-rate of 0.9 times the adiabatic lapse rate is shown in Figure 3.3. This diagram shows the variation of the magnitude of the greenhouse effect with increasing infrared opacity. As one would expect, the magnitude of the greenhouse effect is greater

TABLE 3.3

MAGNITUDE OF GREENHOUSE EFFECT, T_g/T_e, ON VENUS FOR TWO-LAYER MODEL[g]

τ_g	k	p	n	τ_t/τ_g	T_g/T_e	T_g (°K)
2.5	.286	.041	.99	.024	2.49	590
3.0	.25	.026	.99	.013	2.48	588
5.0	.286	.03	.99	.016	2.75	652
6.0	.286	.024	.99	.013	2.95	699
7.0	.25	.014	.99	.007	2.91	690
6.0	.153	7×10^{-4}	.99	$\sim 2\times10^{-4}$	2.94	697
7.0	.153	7×10^{-4}	.99	$\sim 2\times10^{-4}$	2.96	700
8.0	.153	7×10^{-4}	.99	$\sim 2\times10^{-4}$	2.97	704

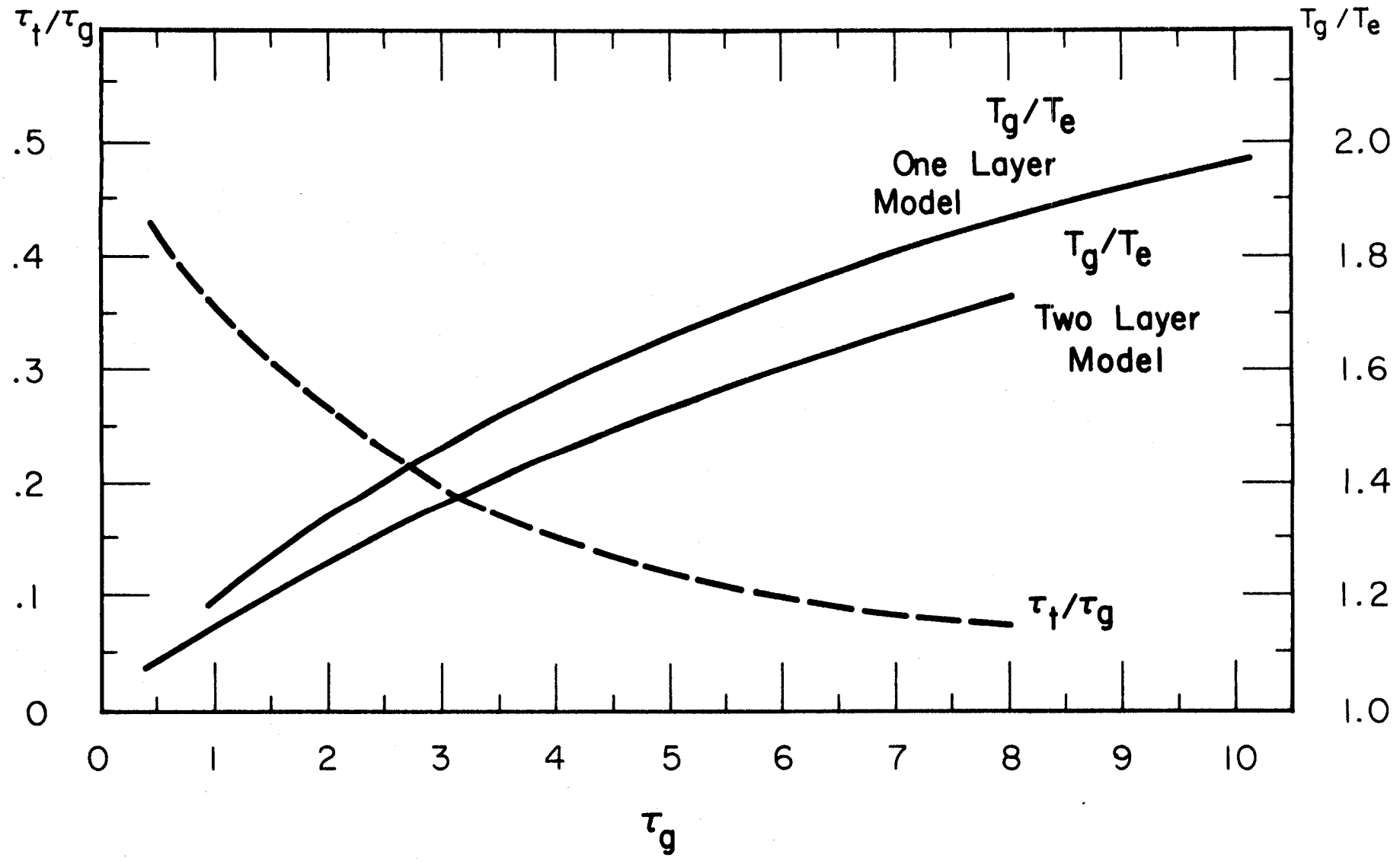

Figure 3.3. Comparison of greenhouse effect for one and two layer models with no clouds and with lapse-rate of 0.9 times adiabatic.

for the one-layer model. Also shown in Figure 3.3 is the variation of τ_t/τ_g, or the ratio of tropopause pressure to surface pressure, with atmospheric infrared opacity, τ_g. The variation is such that as the infrared opacity increases, τ_t/τ_g decreases, and, hence, the tropopause height increases.

We may conclude from the computations with the two-layer model that, as far as the results for Venus are concerned, there is a negligible difference between the one-layer and two-layer greenhouse models.

3.1.5 Application to Other Planets. Since both the one-layer and two-layer models are quite general, they can be applied to other planets; and since there are a number of uncertainties in the models, such application, especially to Mars and Earth, where the values of the parameters are better known, provides a test of the models.

For Mars, the following values for the parameters are assumed: $T_e = 219^oK$ (corresponding to an albedo of 0.15); no clouds; $\tau_g = 0.5$ (after Arking, 1962); and a lapse-rate of nine-tenths of the adiabatic lapse-rate ($k = 0.25$). With the two-layer model, a computation was also made with an adiabatic lapse rate ($k = 0.286$). The results are presented in Table 3.4.

TABLE 3.4

MAGNITUDE OF GREENHOUSE EFFECT ON MARS
FOR ONE-LAYER AND TWO-LAYER MODELS

				One-Layer		Two-Layer		
τ_g	k	n	$T_e(^oK)$	(T_g/T_e)	$T_g(^oK)$	(T_g/T_e)	$T_g(^oK)$	$\tau+/\tau_g$
0.5	0.25	0	219	1.096	240	1.08	237	0.42
0.5	0.286	0	219			1.096	240	0.44

The computed surface temperatures of 237^oK to 240^oK are in reasonable agreement with the estimate of about 230^oK obtained in a more elaborate treatment (Ohring, et al., 1962). The computed surface temperature for the one-layer model is 3^oK higher than for the two-layer model. In the two-layer model, one of the results of the computation is the ratio of tropopause pressure to surface pressure, represented by τ_t/τ_g, which turns out to be about 0.4. In a computation of the average vertical distribution of temperature in the Martian atmosphere (Ohring, 1963), the ratio of tropopause pressure to surface pressure, as determined from the computed temperature versus pressure curve, was found to be about 0.6.

For Earth, the various parameters are specified as follows. The infrared opacity, τ_g, of the atmosphere is taken to be 1.6, which corresponds to an infrared flux transmissivity of 10%. The cloud-tops are assumed to be located at one level in the atmosphere, which is taken to

be 500 mb; hence, p = 0.5. This is an average value based upon an analysis of the climatological cloud statistics presented by London (1957), which led to a value of about 5 km for the average cloud-top height. The average amount of cloudiness is about 50% (London, 1957). With a planetary albedo of 0.35 (London, 1957), T_e is 252°K. Although the observed value of the lapse-rate in the Earth's atmosphere, about 6°K/km, corresponds to a k value of 0.176, computations with the one-layer model were also performed with k = 0.25, corresponding to a lapse-rate of 0.9 times the adiabatic lapse rate. The results of the latter computation might be indicative of uncertainties to be expected in the computations for Mars and Venus, if the actual lapse rates in their atmospheres are substantially different from the ones we assumed. The results of these computations are shown in Table 3.5.

TABLE 3.5

MAGNITUDE OF GREENHOUSE EFFECT ON EARTH
FOR ONE-LAYER AND TWO-LAYER MODELS

					One-Layer		Two-Layer		
τ_g	k	n	p	T_e(°K)	(T_g/T_e)	T_g(°K)	(T_g/T_e)	T_g(°K)	(τ_t/τ_g)
1.6	0.25	0.5	0.5	252	1.33	335			
1.6	0.176	0.5	0.5	252	1.24	313	1.186	299	0.181

The observed average surface temperature for the Earth is 288°K. With the one-layer model and with k = 0.25, the computed surface temperature is quite a bit higher than 288°K. With k = 0.176, the one-layer model predicts 313°K, which, although closer to the observed temperature, is still almost 10% higher. The two-layer model, with k = 0.176, comes closest, as expected, with a temperature of 299°K. These calculations indicate the magnitude of the uncertainties to be expected when the greenhouse model is applied to other planets.

It is of interest to note that the computed ratio of tropopause pressure to surface pressure for the two-layer model, (τ_t/τ_g), is 0.181. This is in good agreement with the observed average value of about 0.2 in the Earth's atmosphere.

For the Earth, another set of computations was performed. The purpose of these computations was to estimate the average surface temperature under different conditions of average cloud amount. Cloud amount has a dual influence on surface temperature. For example, an increase in the amount of cloudiness will, on the one hand, increase the Earth's planetary albedo, thus causing a decrease in the amount of solar radiation available to heat the Earth, which would lead to a decrease in average surface temperature, and, on the other hand, increase the magnitude of the greenhouse effect, which would lead to an increase of average surface temperature. It is of interest to estimate the changes in average surface temperature that would occur

if the average amount of cloudiness was changed substantially from its present value of about 50%. In particular, we shall determine the average surface temperature for 90% cloudiness, and for no clouds or totally clear skies.

For the present average amount of cloudiness, 50%, the planetary albedo is 35%, and for totally clear skies, the planetary albedo is 15%; both of these values are based upon computations by London (1957). The planetary albedo for the case of 90% cloudiness is assumed to be 50%, based upon an extrapolation of the albedo for no clouds and the albedo for 50% cloudiness. The amounts of cloudiness and the corresponding planetary albedos are shown in Table 3.6.

TABLE 3.6

Amount of cloudiness (%)	0	50	90
Planetary albedo (%)	15	35	50

For these computations, it is assumed that there are no changes in atmospheric infrared opacity, in temperature lapse-rate in the troposphere, and in the height of the cloud-tops; these parameters are assumed to remain constant at their present values of $\tau_g = 1.6$, $\frac{dT}{dz} = -6.0^{\circ}K/km$ ($k = 0.176$), and $p = 0.5$, as the amount of cloudiness changes. The results of these computations, and the computation for present average cloudiness, are shown in Table 3.7.

TABLE 3.7

CHANGES IN THE AMOUNT OF CLOUDINESS AND THE AVERAGE SURFACE TEMPERATURE OF THE EARTH

Amount of Cloudiness (%)	T_g/T_e	T_e (^oK)	T_g (^oK)	τ_t/τ_g
0	1.13	270	305	0.263
50	1.186	252	299	0.181
90	1.23	236	290	0.131

If the cloud amount is increased to 90%, we note, from Table 3.7, that the surface temperature would be 290^oK; this represents a decrease of 9^oK from the computed value of the present average surface temperature. If all clouds are eliminated from the atmosphere, the surface temperature would be 305^oK; this represents an increase of 6^oK above the computed value of the present average surface temperature. Thus, it appears that even with quite dramatic changes in the amount of cloudiness, the Earth's average surface temperature would change by less than 10^oK. This is due to the opposite effects that cloudiness has on the average surface temperature.

The last column of Table 3.7 shows the computed variation with cloudiness of the ratio of tropopause pressure to surface pressure. This is seen to decrease with increasing cloudiness.

More detailed computations of changes in the Earth's surface temperature as a result of changes in average cloud amount would have to

consider the changes in atmospheric water vapor content, vertical temperature structure, and average height of clouds that would probably accompany large scale changes in the total amount of clouds. However, the present computations do yield some insight on the effect of changes in cloudiness on the Earth's surface temperature, and should be useful in studies of climatic change.

3.2 ABSORPTION OF SOLAR RADIATION BY CARBON DIOXIDE IN THE VENUS ATMOSPHERE

3.2.1 Introduction. In greenhouse models of the Venus atmosphere, it is generally implicitly assumed that the portion of the solar radiation that is not reflected back to space reaches the surface of the planet. Actually, however, some of the radiation is probably absorbed in the very thick atmosphere of the planet, and in the cloud layer. Since the composition of the cloud layer is unknown, it is difficult to estimate how much depletion of the solar beam takes place in the clouds. Estimates of direct absorption by the atmosphere are also difficult since the atmospheric composition is uncertain, carbon dioxide being the only gas definitely detected. In this section, we attempt to estimate the amount of solar radiation absorbed by the near-infrared bands of carbon dioxide in the Venus atmosphere.

3.2.2 Methodology. Howard, Burch and Williams (1956) have presented empirical formulas relating absorption to path length and pressure for several CO_2 bands. For weak absorption by a minor atmospheric constituent, the empirical equations are of the form

$$A = \int_{\nu_1}^{\nu_2} A_\nu \, d\nu = c \, [up^{2k}]^{1/2} \qquad (3.21)$$

where A is the band absorption, A_ν is the absorption at wavenumber ν, u is the absorber path length in cm NTP, and p is the atmospheric pressure

in mm Hg. The values of the empirical constants c and k vary from band to band. For stronge absorption (where $\int_{\nu_1}^{\nu_2} A_\nu \, d\nu$ is greater than an empirical value that varies from band to band) they obtained

$$A = \int_{\nu_1}^{\nu_2} A_\nu \, d\nu = C + D \log up^{K/D} \qquad (3.22)$$

The empirical constants for the different bands of interest of this study are shown in Table 3.8.

The column labelled "Determining A" provides the basis for using either the weak or strong fit.

A model atmosphere has been constructed for Venus by Kaplan (1963), and this can be used to obtain an estimate of the total CO_2 path length u. The path length can be determined from

$$u = \frac{m_c}{m_v} \frac{\int_o^\infty \rho_c \, dz}{\rho_c'} = \frac{m_c}{m_v} \left(\frac{1}{\rho_c'}\right)\left(\frac{\rho_c}{\rho_v}\right)\frac{1}{g} p_o \qquad (3.23)$$

where m_c is the molecular weight of carbon dioxide, m_v is the molecular weight of the Venus atmosphere, ρ_c is the density of carbon dioxide, ρ_c' is the density of CO_2 at STP, (ρ_c/ρ_v) is the volume percentage of CO_2, g is gravity, and p_o is surface pressure. Using the values $m_c = 44$; $m_v = 29.6$; $\rho_c' = 1.94 \times 10^{-3}$ g cm^{-3}; $(\rho_c/\rho_v) = 0.10$; g = 900 cm sec^{-2}; and $p_o = 10$ atm = 10^7 dynes cm^{-2}, we obtain $u = 1.1 \times 10^6$ cm STP.

TABLE 3 8

EMPIRICAL RELATIONS FOR CO_2 BANDS

Band (μ)	Band Limits (cm^{-1})	Weak Fit C	K	Determining A (cm^{-1})
5.2	1870 - 1980	.024	.40	< 30
4.8	1980 - 2160	.12	.37	60
4.3	2160 - 2500	--	--	50
2.7	3480 - 3800	3.15	.43	50
2.0	4750 - 5200	.492	.39	80
1.6	6000 - 6550	.063	.38	80
1.4	6650 - 7250	.058	.41	80

Band (μ)	Band Limits (cm^{-1})	Strong Fit C	D	K
4.3	2160 - 2500	27.5	34	31.5
2.7	3480 - 3800	-137.0	77	68.0
2.0	4750 - 5200	-536.0	138	114.0

Examination of Equation (3.21) for the weak fit and the weak fit part of Table 3.8 reveals that, with this much carbon dioxide and with the pressures prevailing on Venus, the strong fit must be used for all the carbon dioxide bands. Unfortunately, several of the bands do not have strong fit relations. However, King (1963) has developed a theoretical relationship between some of the constants in the strong and weak fits, and we can use this relationship to obtain an estimate of the necessary strong fits. King's relationship is

$$\log .8686\ D + \frac{C}{2D} = -.4343\delta \qquad (3.24)$$

where $\delta = 0.981$

Thus, given D and C one can estimate c. However, we would like to obtain estimates of D and C, given c. In order to accomplish this, we have assumed that there is an approximate relationship between D and C of the form $D = a + b\ C$. From Howard et al's values of D and C for CO_2 bands, we have determined, by a least squares procedure, the relationship

$$D = 43.9 - .180\ C \qquad (3.25)$$

By substituting this relation in Equation (3.24) we now have a means of determining C (the strong fit constant) from c (the weak fit constant). This has been done for the 5.2μ, 4.8μ, 1.6μ, and 1.4μ bands, and these results as well as the Howard et al results for 4.3μ, 2.7μ, and 2.0μ are shown in Table 3.9.

TABLE 3 9

STRONG FIT RELATIONS FOR CO_2 BANDS

Band (μ)	Band Limits (cm^{-1})	C	D	K
5.2	1870 - 1980	-49.5	52.8	----
4.8	1980 - 2160	-243.0	87.6	----
4.3	2160 - 2500	27.5	34.0	31.5
2.7	3480 - 3800	-137.0	77.0	68.0
2.0	4750 - 5200	-536.0	138.0	114.0
1.6	6000 - 6550	-137.0	68.6	----
1.4	6650 - 7250	-127.0	66.0	----

The values for 4.3μ, 2.7μ, and 2.0μ indicate that the ratio K/D, needed for Equation (3.22), is about 0.9. We have therefore assumed that K/D is equal to 0.9, independent of band.

We can write Equation (3.22) in the following form

$$A = C + D \log u_r \tag{3.26}$$

where $u_r = up^{K/D}$ for a path at constant pressure, and $u_r = \int_{u(p_1)}^{u(p_2)} p^{K/D}\, du$ for a path through an atmosphere with varying pressure. For the atmosphere of Venus, we must use the second relationship for u_r. Since the CO_2 mixing ratio is constant with altitude, the CO_2 path length is directly proportional to pressure, and we have $u = \alpha p$, $du = \alpha dp$, and $u_o = \alpha p_o$, where u_o is the total CO_2 path length, and p_o is surface pressure.

Then

$$u_r = \alpha \int_o^{p_o} p^{K/D}\, dp \tag{3.27}$$

Integration of this expression yields

$$u_r = \frac{u_o\, p_o^{K/D}}{(K/D) + 1}$$

With $u_o = 1.1 \times 10^5$ cm STP, $p_o = 7.6 \times 10^3$ mm, and K/D = 0.9, the reduced path length is equal to 9×10^8.

3.2.3 Computations and Results. The absorption A can now be computed for each of the bands in Table 3.9 with the use of Equation (3.26). The fractional absorption of each of these bands can be obtained from

$$a = \frac{A}{\Delta\nu}$$

where $\Delta\nu$ is the width of the band in cm^{-1}. The computed values of fractional absorption, a, are shown in Table 3.10.

Since the real value of the fractional absorptivity cannot be greater than unity, all bands with computed values of a greater than one were assumed to have fractional absorptivities of unity.

In order to compute the absorption of solar radiation in the Venus atmosphere by these CO_2 bands, we must first determine the amount of solar energy available for absorption. This amount depends essentially upon Venus' distance from the Sun, and the planetary albedo at the different wavelengths. Table 3.11 indicates the solar radiation intensities, albedos, available radiation intensities, absorptivities, and, finally, absorbed energy values for each of the CO_2 bands. The solar radiation intensities are based upon a $6000^{o}K$ blackbody Sun, a fair approximation in the near infrared. The albedos are after Sinton (1962). The last figure in the last column is the total amount of solar radiation absorbed in the Venus atmosphere by these CO_2 bands. Since the total solar insolation at the top of the atmosphere is about 2650 watts m^{-2}, the CO_2 absorption amounts to over 3% of this value. The integrated planetary

TABLE 3.10

FRACTIONAL ABSORPTION BY CO_2 BANDS

Band (μ)	a(computed)	a(adopted)
5.2	3.8	1.0
4.8	3.0	1.0
4.3	0.98	0.98
2.7	1.7	1.0
2.0	1.56	1.0
1.6	0.87	0.87
1.4	0.79	0.79

TABLE 3 11

COMPUTATION OF CO_2 ABSORPTION IN VENUS ATMOSPHERE

Band (μ)	$\Delta\lambda$ ($m\mu$)	Intensity Outside Atmosphere I(watts m^{-2})	Albedo A	Available Energy (1 - A)I	Absorptivity a	CO_2 Absorption a(1 - A)I watts m^{-2}
5.2	5348-5051	1.9	.15	1.6	1.0	1.6
4.8	5051-4630	3.7	.15	3.1	1.0	3.1
4.3	4630-4000	8.5	.15	7.2	0.98	7.1
2.7	2874-2632	10.2	.15	8.7	1.0	8.7
2.0	2105-1923	37.4	.40	22.4	1.0	22.4
1.6	1667-1527	59.9	.52	28.8	0.87	25.1
1.4	1504-1379	76.7	.75	19.2	0.79	15.2
						83.2

albedo of Venus is about 0.73 (Sinton, 1962), so that, after correcting for albedo losses, the amount of energy remaining before absorption processes is about 715 watts m^{-2}. The CO_2 absorption, 83.2 watts m^{-2}, is about 12% of this value.

We may conclude from these estimates that the assumption that all of the unreflected solar radiation reaches the surface of Venus is in error by at least 12%, since CO_2 alone is capable of absorbing this amount. Absorption by the clouds and other atmospheric constituents would increase this figure.

3.3 RADIATIVE EQUILIBRIUM DISTRIBUTION OF TEMPERATURE BELOW THE VENUS CLOUD LAYER

3.3.1 Introduction. Observational evidence indicates that the planet Venus is covered by an extensive cloud layer. It is of interest to attempt a theoretical determination of the vertical variation of temperature between the surface of the planet and the base of the cloud layer. Estimates are available for the surface temperature and the cloud temperatures. If we assume that the atmosphere between the cloud base and surface is in infrared radiative equilibrium, we can compute a radiative equilibrium temperature distribution between these two levels. The computed temperature distribution may serve as a useful estimate of the actual temperature distribution, if the assumption and model used for the computations are not too unrealistic. In this section, we develop a technique for making this kind of computation, and apply it to the atmosphere of Venus.

3.3.2 Methodology. It is assumed that the cloud layer completely covers the sky and that both the cloud base and planetary surface radiate as blackbodies at fixed temperatures. It is further assumed that the atmospheric layer between the cloud base and planetary surface is a grey absorber and is in infrared radiative equilibrium. The net infrared flux at any opacity level τ within this atmospheric layer can then be written as

$$F(\tau) = 2B(o)E_3(\tau) - 2B(b)E_3(\tau_b - \tau) + 2\int_o^{\tau} B(t)E_2(\tau - t)dt - 2\int_{\tau}^{\tau_b} B(t)E_2(t - \tau)dt \qquad (3.28)$$

where $\tau = \int_o^z k\rho dz$, k being the grey absorption coefficient, ρ the density of the absorbing gas, and z the height; B(o) is the blackbody radiation flux from the surface; B(b) is the blackbody radiation flux from the cloud base; B(t) is the blackbody flux at any level within the atmosphere; and E's are exponential integrals. The infrared opacity is taken as zero at the surface, increasing to τ_b at the cloud base (see sketch).

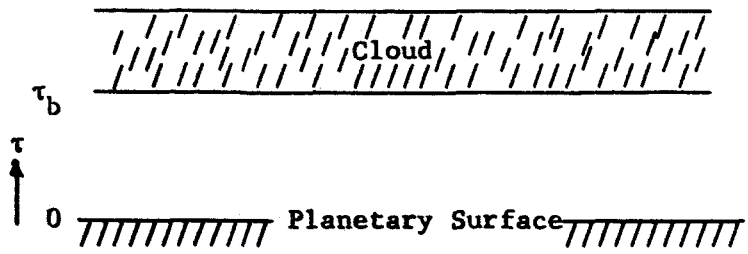

Under conditions of radiative equilibrium $\frac{dF}{d\tau} = 0$. Differentiating Equation (3.28) with respect to τ, one obtains

$$\frac{dF}{d\tau} = -B(b)E_2(\tau_b - \tau) - B(o)E_2(\tau) - \int_o^{\tau} B(t)E_1(\tau - t)dt - \int_o^{\tau_b} B(t)E_1(t - \tau)dt + 2\,B(\tau). \qquad (3.29)$$

Setting this expression equal to zero and solving for $B(\tau)$, one obtains

$$B(\tau) = \frac{1}{2}\left[B(o)E_2(\tau) + B(b)E_2(\tau_b - \tau) + \int_o^{\tau_b} B(t)E_1(|\tau - t|)dt\right] \qquad (3.30)$$

This equation can be written in terms of temperature with the use of the relationship $B = \sigma T^4$; one then obtains

$$T^4(\tau) = \frac{1}{2}\left[T^4(o)E_2(\tau) + T^4(b)\ E_2(\tau_b - \tau) + \int_o^{\tau_b} T^4(t)E_1(|\tau - t|)dt\right] \tag{3.31}$$

We would like to obtain $T(\tau)$ from this equation, given $T^4(o)$, $T^4(b)$, and τ_b. The following discussion indicates the numerical techniques used to obtain the required variation of temperature with τ.

The object is to solve the second order integral equation,

$$T^4(\tau) = A(\tau) + \int_o^{\tau_b} \epsilon(\tau,t)T^4(t)dt \tag{3.32}$$

where

$$A(\tau) = \frac{1}{2}\left[T^4(o)E_2(\tau) + T^4(\tau_b)E_2(\tau_b - \tau)\right]$$

and

$$\epsilon(\tau,t) = \frac{1}{2}\left[E_1(|\tau - t|)\right]$$

for $T(\tau)$, the temperature in degrees Kelvin, at the point, τ, and obtain a temperature distribution in the interval, $o \leq \tau \leq \tau_b$.

The usual procedure for solving this type of equation is to consider a discrete set of points (τ_1, τ_2, ... τ_n) in the interval, $o \leq \tau \leq \tau_b$, and to approximate the integral Equation (3.32) at each point τ_i, as the sum,

$$T^4(\tau_i) = A(\tau_i) + \sum_{j=1}^{n} \epsilon(\tau_i, \tau_j) T^4(\tau_j) D(\tau_j), \quad (i = 1, 2, ..., n) \tag{3.33}$$

where $D(\tau_j)$ is a function of the interval $\Delta\tau_j = \tau_{j+1} - \tau_j$, depending on the method used for approximating the integral of Equation (3.32).

This procedure reduces the problem to solving the following matrix equation,

$$\begin{pmatrix} T_1 \\ T_2 \\ \vdots \\ T_n \end{pmatrix} = \begin{pmatrix} A_1 \\ A_2 \\ \vdots \\ A_n \end{pmatrix} + \begin{pmatrix} \epsilon_{11}D_1 & \epsilon_{12}D_2 & \cdots\cdots & \epsilon_{1n}D_n \\ \epsilon_{21}D_1 & \epsilon_{22}D_2 & \cdots\cdots & \epsilon_{2n}D_n \\ \vdots & & & \\ \epsilon_{n1}D_1 & \epsilon_{n2}D_2 & \cdots\cdots & \epsilon_{nn}D_{nn} \end{pmatrix} \begin{pmatrix} T_1 \\ T_2 \\ \vdots \\ T_n \end{pmatrix} \tag{3.34}$$

where

$$A_i = A(\tau_i)$$

$$\epsilon_{ij} = \epsilon(\tau_i, \tau_j)$$

$$T_i = T^4(\tau_i)$$

Difficulty arises in evaluating Equation (3.34) for T_i, however, because the diagonal elements of the kernal are singular, i.e.

$$\epsilon_{ii} = \frac{1}{2} E_1(|\tau_i - \tau_i|) = \frac{1}{2} E_1(o) = \infty \tag{3.35}$$

In the present problem, this anomaly was eliminated by slightly modifying the above procedure. The method is outlined below.

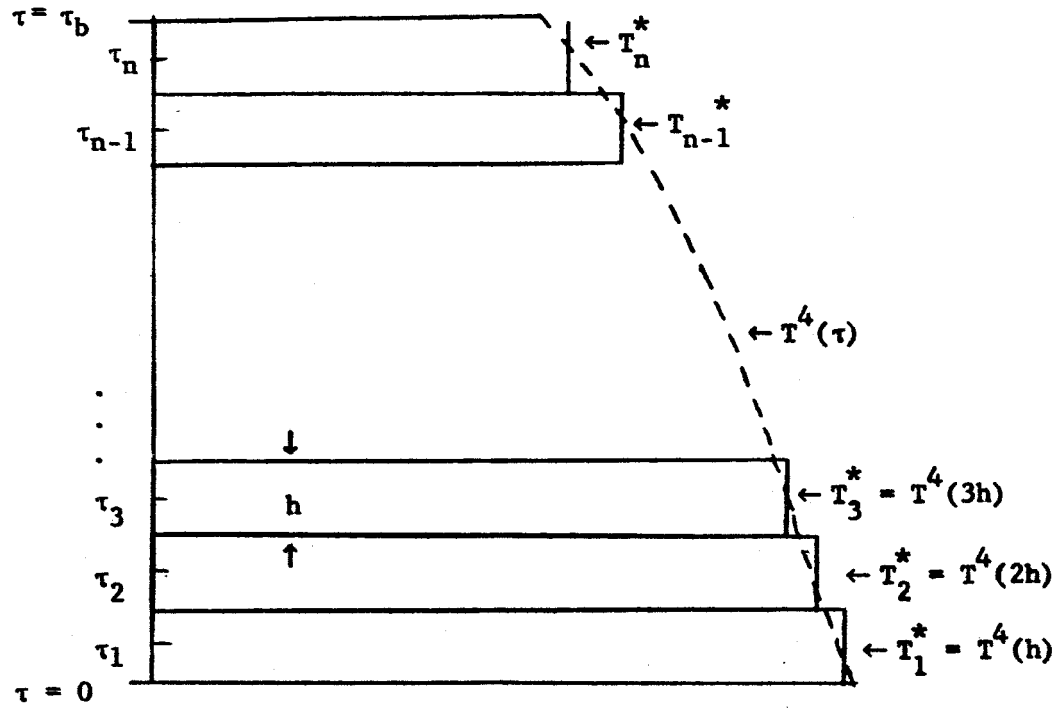

Instead of attempting to evaluate the temperature at certain points in the interval $0 \leq \tau \leq \tau_b$, the interval is divided into equal segments of length, h, (see sketch), and the temperature is considered constant in each segment. This assumption is justified since the function $T(\tau)$ is regular in the interval, and the segment, h, can be made small enough such that the change in temperature within any segment is negligible.

Thus, with $T(\tau)$ constant in each segment, the integral of Equation (3.32) can be directly integrated over each segment, and the matrix Equation (3.34) reduces to the following:

$$\begin{pmatrix} T_1^* \\ \vdots \\ T_n^* \end{pmatrix} = \begin{pmatrix} A_1^* \\ \vdots \\ A_n^* \end{pmatrix} + \begin{pmatrix} \frac{1}{2}\int_0^h E_1(|\tau_1 - t|)dt & \cdots & \frac{1}{2}\int_{(n-1)h}^{nh=\tau_b} E_1(t-\tau_1)dt \\ \vdots & & \vdots \\ \frac{1}{2}\int_0^h E_1(\tau_n - t)dt & \cdots & \frac{1}{2}\int_{(n-1)h}^{nh=\tau_b} E_1(|\tau_n - t|)dt \end{pmatrix} \begin{pmatrix} T_1^* \\ \vdots \\ T_n^* \end{pmatrix} \tag{3.36}$$

where,

$$T_k^* = T^4(kh)$$

$$A_k^* = \frac{1}{2}\left\{T^4(o)E_2[(k - \tfrac{1}{2})h] + T^4(\tau_b)E_2[(n - k + \tfrac{1}{2})h]\right\}$$

Integrating the elements of the kernal matrix, and denoting them by K_{ij},

$$K_{ii} = \frac{1}{2}\int_{(i-1)h}^{ih} E_1(|\tau_i - t|)dt = \frac{1}{2}\int_{(i-1)h}^{(i-\frac{1}{2})h} E_1(\tau_i - t)dt + \frac{1}{2}\int_{(i-\frac{1}{2})h}^{ih} E_1(t-\tau_i)dt$$

$$= \tfrac{1}{2}E_2(o) - \tfrac{1}{2}E_2(\tfrac{1}{2}h) - \tfrac{1}{2}E_2(\tfrac{1}{2}h) + \tfrac{1}{2}E_2(o)$$

$$= 1 - E_2(h/2)$$

$$K_{ij} = \frac{1}{2}\int_{(j-1)h}^{jh} E_1(\tau_i - t)dt = \frac{1}{2}\left\{E_2[\tau_i - jh] - E_2[\tau_i - (j-1)h]\right\} \quad i > j$$

$$K_{ij} = \frac{1}{2} \int_{(j-1)h}^{jh} E_1(t-\tau_i)\,dt = \frac{1}{2} \left\{ E_2[(j-1)h - \tau_i] - E_2[jh - \tau_i] \right\} \quad i < j$$

The solution is,

$$\begin{pmatrix} T_1^* \\ T_2^* \\ \vdots \\ T_n^* \end{pmatrix} = \begin{pmatrix} 1-K_{11} & -K_{12} & \cdots & -K_{1n} \\ -K_{21} & 1-K_{22} & \cdots & -K_{2n} \\ \vdots & & & \vdots \\ -K_{n1} & -K_{n2} & & 1-K_{nn} \end{pmatrix}^{-1} \begin{pmatrix} A_1^* \\ A_2^* \\ \vdots \\ A_n^* \end{pmatrix} \tag{3.37}$$

A program has been constructed to evaluate Equation (3.37) **for as many as fifteen segments, giving numerical values of T_i^* with seven place accuracy.**

3.3.3 Computations and Results. The surface temperature is taken as 700°K, based upon the radio-wavelength emission observations. The cloud-base temperature is taken as 373°K (100°C) based upon the value of about 200°F (366°K) given in the report, Mariner: Mission to Venus. This value is only an estimate, since the cloud-base temperature has never been measured. The only other parameter that must be specified before computations can be performed is the infrared opacity of the atmosphere between the surface and the cloud-base. Since this parameter is unknown, we have performed computations for a range of τ_b values, including τ_b = 1, 2, 3, 5, and 10. The atmospheric layer is broken up into 15 intervals, and temperatures are computed for each interval. The results are presented in Table 3.12. In this table the τ values are mid-points of the layers for which the temperatures were computed.

Table 3.12. Radiative equilibrium temperatures below the cloud on Venus.

	$\tau_b = 1$		$\tau_b = 2$		$\tau_b = 3$		$\tau_b = 5$		$\tau_b = 10$	
	τ	T(^{o}K)	τ	T(^{o}K)	τ	T(^{o}K)	τ	T(^{o}K)	τ	T(^{o}K)
Ground	0	700	0	700	0	700	0	700	0	700
	.03	653	.07	665	.10	672	.17	678	.33	685
	.10	645	.20	656	.30	662	.50	668	1.00	674
	.17	637	.33	647	.50	652	.83	658	1.67	663
	.23	630	.47	638	.70	643	1.17	647	2.33	652
	.30	623	.60	629	.90	633	1.50	636	3.00	640
	.37	615	.73	620	1.10	622	1.83	625	3.67	628
	.43	608	.87	610	1.30	612	2.17	613	4.33	614
	.50	600	1.00	600	1.50	600	2.50	600	5.00	600
	.57	592	1.13	590	1.70	588	2.83	586	5.67	585
	.63	584	1.27	578	1.90	575	3.17	572	6.33	568
	.70	575	1.40	566	2.10	561	3.50	556	7.00	550
	.77	565	1.53	553	2.30	546	3.83	538	7.67	530
	.83	554	1.67	539	2.50	529	4.17	518	8.33	507
	.90	543	1.80	522	2.70	510	4.50	496	9.00	480
	.97	529	1.93	503	2.90	487	4.83	468	9.67	447
Cloud-base	1.00	373	2.00	373	3.00	373	5.00	373	10.00	373

For a grey atmosphere, the infrared opacity is proportional to the pressure, and we can determine the temperature distribution as a function of atmospheric pressure. We take the value $p = 2 \times 10^{-1}$ atm for the pressure at the cloud base; this value is based upon our temperature of 373°K and the temperature - pressure model atmosphere presented by Kaplan (1963). For the pressure at the surface, we take the value 10 atm, again based upon Kaplan's (1963) model.

For a grey atmosphere, we have

$$d\tau = \alpha \rho \, dz = - \frac{\alpha}{g} dp \tag{3.38}$$

where τ is infrared opacity, α is the grey absorption coefficient of the atmosphere, ρ is density of the atmosphere, z is height, and p is pressure. Therefore,

$$d\tau = - A \, dp \tag{3.39}$$

or

$$\tau = - A p + B \tag{3.40}$$

where $A = \left(\frac{\alpha}{g} \right)$ and B is a constant. A and B can be determined from the conditions $\tau = \tau_b$ at $p = 2 \times 10^{-1}$ atm, and $\tau = 0$ at $p = 10$ atm. The resulting relationship is

$$p = \frac{10 \, \tau_b - 9.8 \, \tau}{\tau_b} . \tag{3.41}$$

This permits conversion of opacity (τ) values to pressures (p). We have

plotted the computed temperatures versus pressure on a semi-log scale, and these distributions are shown as Figures 3.4 to 3.8. The semi-log scale is approximately equal to a linear height scale. On each diagram an adiabatic curve is also plotted from the relationship

$$\left(\frac{T}{T_o}\right) = \left(\frac{p}{p_o}\right)^{0.286} \tag{3.42}$$

In general, the computed temperature curves are characteristically super-adiabatic in the atmospheric layer closest to the planet's surface and in the layer immediately below the cloud top. This is not surprising, for previous radiative equilibrium computations have shown that there is a discontinuity in temperature between the surface and atmosphere at the boundary of a layer in radiative equilibrium (See, for example, Goody, 1954). As the infrared opacity, τ_b, increases, the depth of the layers with super-adiabatic lapse rates decreases, and the lapse rates in these layers approach the adiabatic lapse-rate. Layers in which super-adiabatic lapse rates are present are inherently unstable, and convection and mixing will effect a redistribution heat energy such that the final lapse rates in these layers will not be super-adiabatic. Therefore, in those layers in which the computed lapse rates are super-adiabatic, the actual lapse-rates are probably close to adiabatic. In those layers in which the computed lapse rate is sub-adiabatic, and this includes most of the atmosphere between the surface and the cloud-base, the actual temperatures should be quite similar to the computed temperatures.

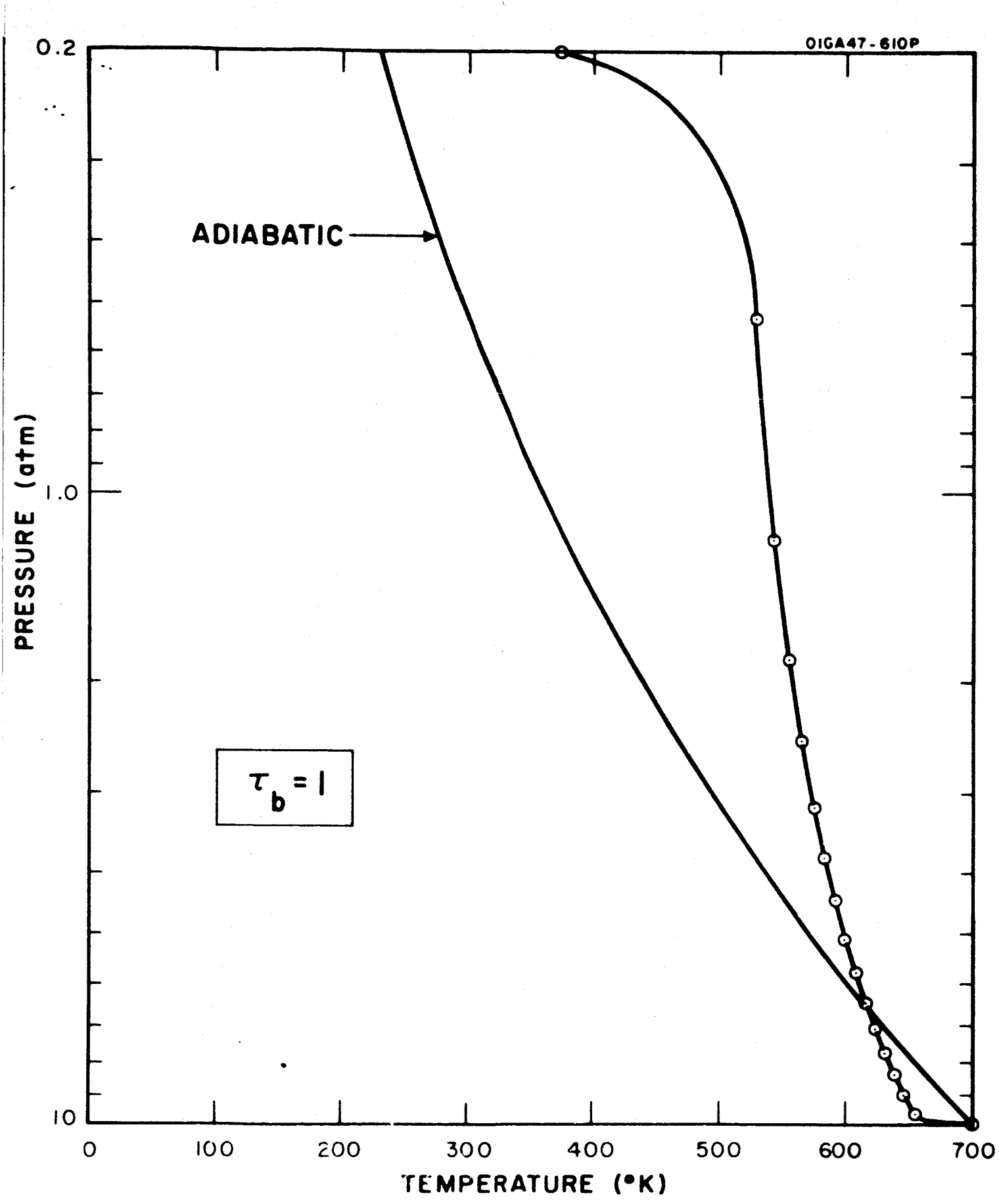

Figure 3.4. Computed radiative equilibrium temperature distribution between surface and cloud-base on Venus for atmospheric infrared opacity of 1. Adiabatic temperature distribution is also shown.

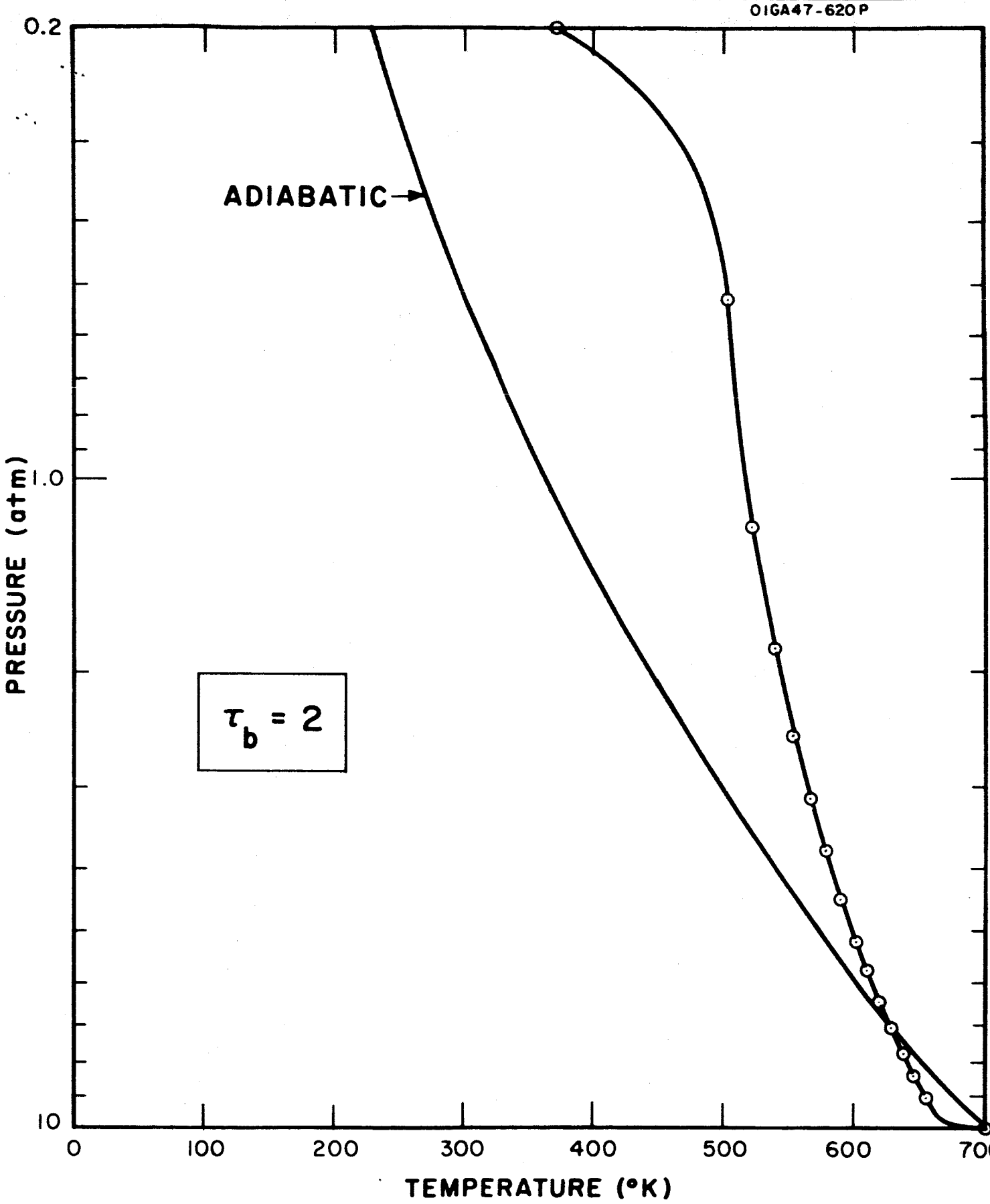

Figure 3 5. Computed radiative equilibrium temperature distribution between surface and cloud-base on Venus for atmospheric infrared opacity of 2. Adiabatic temperature distribution is also shown.

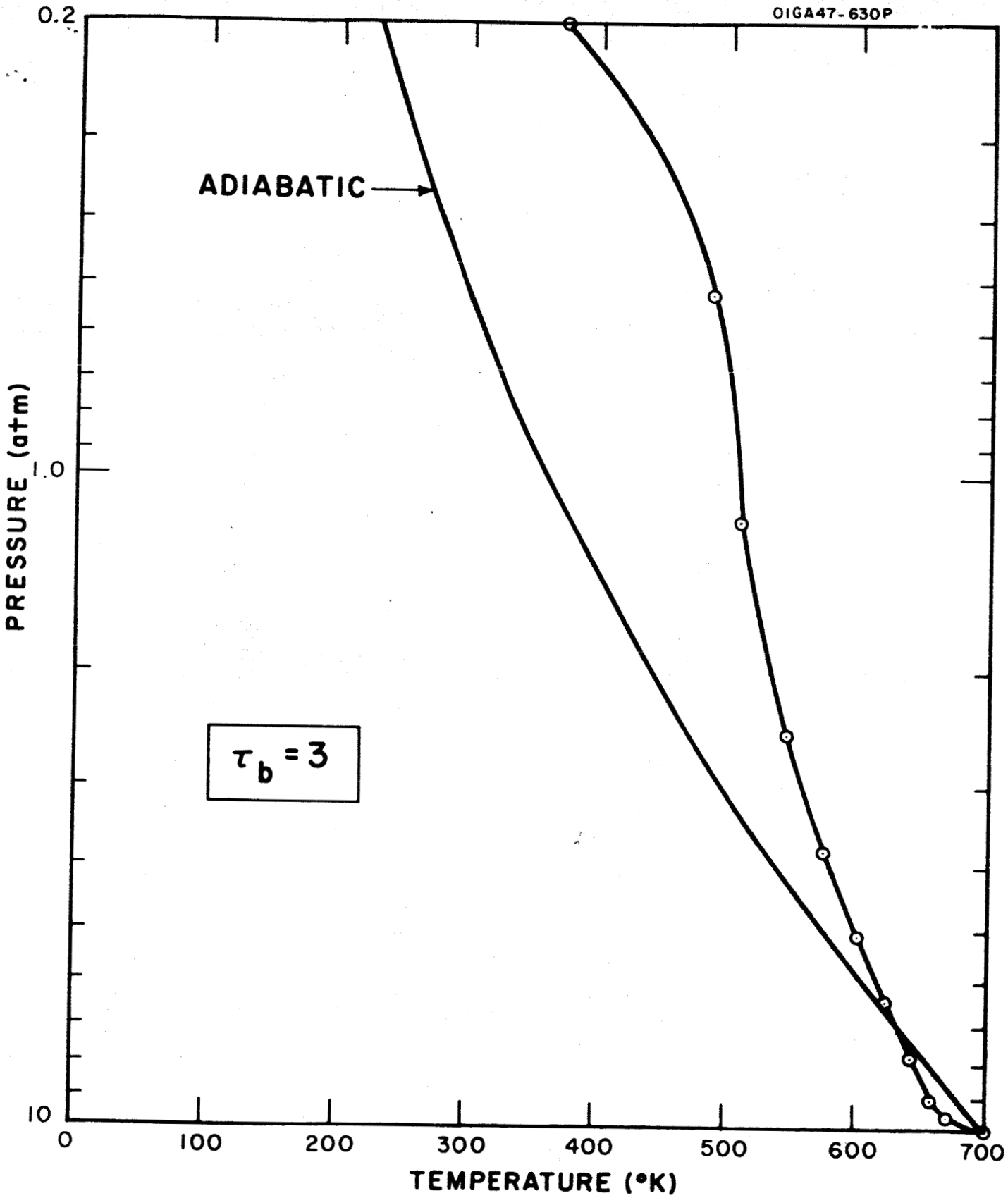

Figure 3.6. Computed radiative equilibrium temperature distribution between surface and cloud-base on Venus for atmospheric infrared opacity of 3. Adiabatic temperature distribution is also shown.

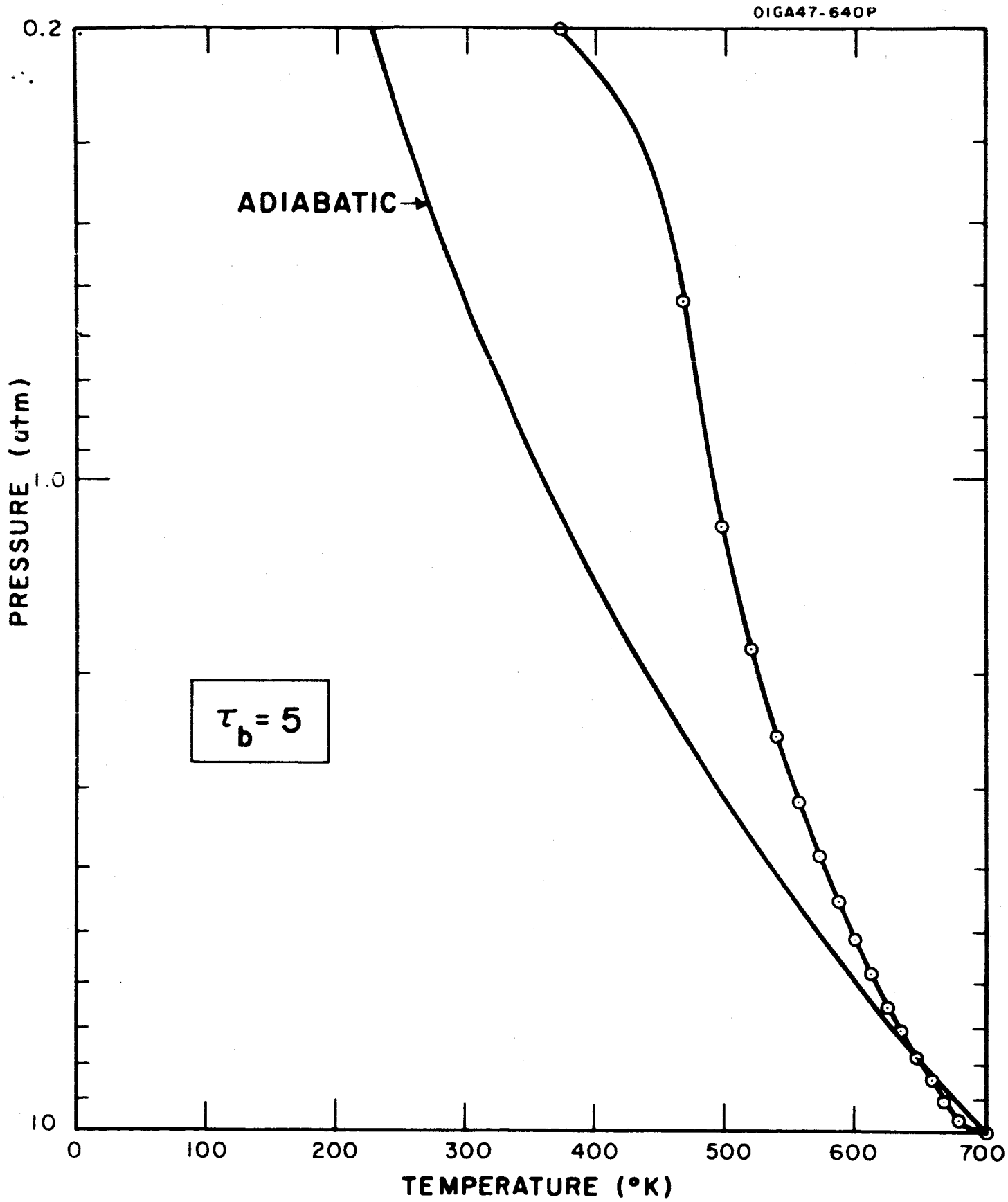

Figure 37. Computed radiative equilibrium temperature distribution between surface and cloud-base on Venus for atmospheric infrared opacity of 5. Adiabatic temperature distribution is also shown.

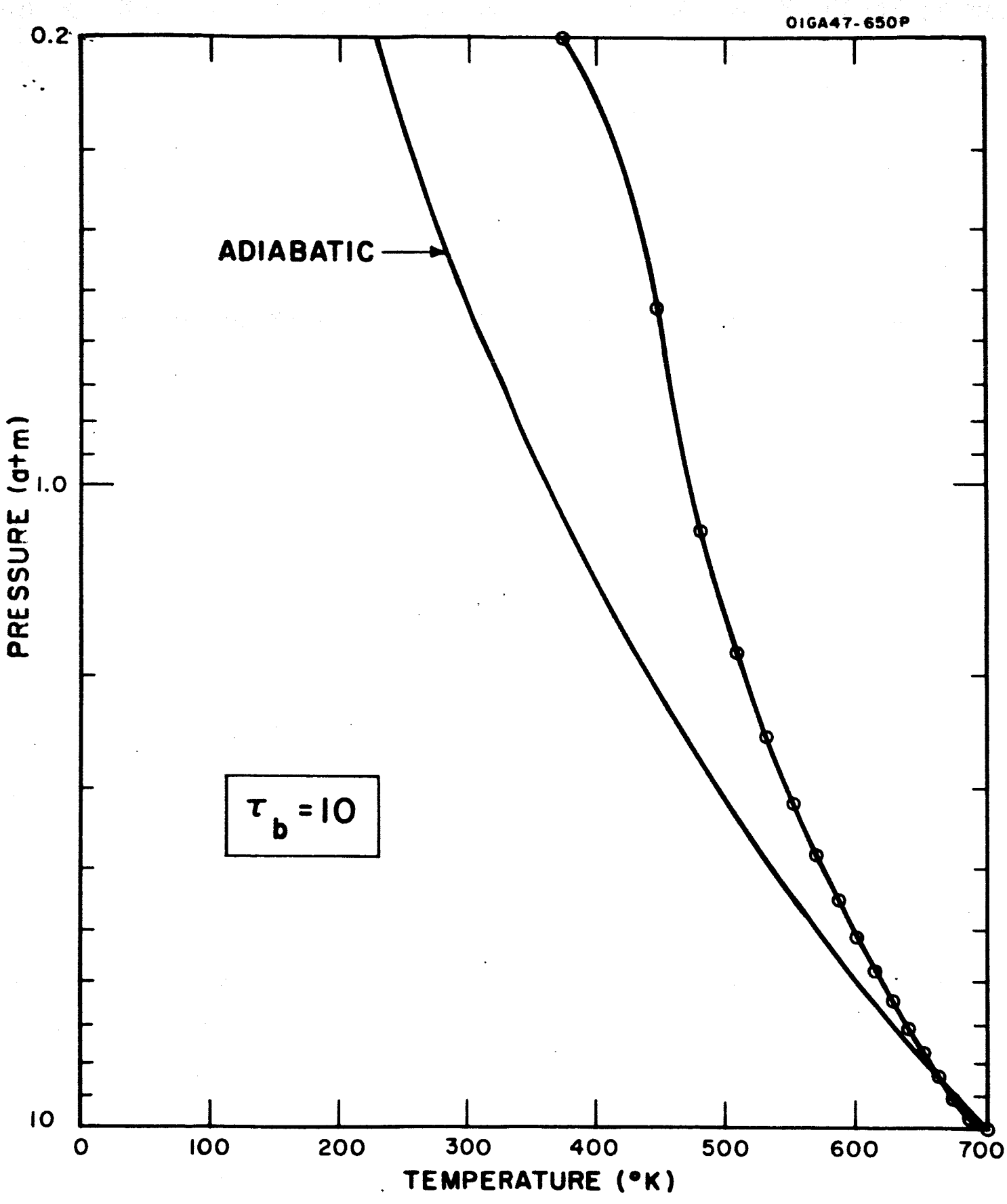

Figure 3.8. Computed radiative equilibrium temperature distribution between surface and cloud-base on Venus for atmospheric infrared opacity of 10. Adiabatic temperature distribution is also shown.

The actual value of the infrared opacity, τ_b, between the cloud-base and the surface of the planet is unknown. Computations of the greenhouse effect in the Venus atmosphere (Ohring and Mariano, 1964) indicate that, with 99% cloudiness, infrared opacities of 6 or 7 for the entire atmosphere are required to maintain a surface temperature of $700^{o}K$. Since the cloud base is located at 2×10^{-1} atm, which is 2×10^{-2} of the surface pressure, most of the atmosphere is below the cloud base. Consequently, the infrared opacity of the entire atmosphere is a fairly good value for the infrared opacity of the sub-cloud layer. Therefore, the actual temperature profile might best be represented by a profile intermediate between those computed for $\tau_b = 5$ and $\tau_b = 10$.

The radiative equilibrium temperature profiles computed in this study can be considered first approximations to the actual vertical temperature structure below the Venus cloud cover. The closeness of the approximation to the actual temperature structure depends upon a number of factors. These include the reality of the physical model used in the computations and the extent to which the atmosphere below the clouds is in infrared radiative equilibrium.

3.4 SUMMARY AND RECOMMENDATIONS

Emphasis was placed on the following three topics related to the meteorology of the Venus atmosphere — (1) further improvement of the greenhouse model for the Venus atmosphere, (2) the amount of solar radiation reaching the surface of Venus, and (3) the vertical temperature distribution between the surface of the planet and the base of the cloud layer.

Two improvements were made in the original greenhouse model. The original computations were performed with the assumption that the temperature lapse-rate in the Venus atmosphere is constant with altitude and is equal to nine-tenths of the adiabatic lapse-rate. The use of this particular lapse-rate permitted an anlytical integration of the radiative transfer equation. The greenhouse equation has now been programmed for an IBM 1620 computer is such a manner that any lapse-rate can be assumed, the integrations now being performed numerically. In particular, computations have been performed for the case of an adiabatic lapse-rate. Another improvement concerns the assumption of a constant temperature lapse-rate throughout the atmosphere. From analogy with the Earth's atmosphere, and on the basis of radiative considerations, one can argue that the temperature does not continue to decrease indefinitely with height. We have therefore developed a two-layer greenhouse model in which the lapse-rate is constant in the lower layer and equal to zero in the upper layer. The height at which the temperature starts to remain

constant with altitude is predicted by the model, which assumes that the upper layer is in radiative equilibrium.

These improvements permit computation of the greenhouse effect for any partially cloudy atmosphere that has a troposphere with arbitrary constant lapse-rate of temperature and an isothermal stratosphere in gross radiative equilibrium. Computations have been performed from Venus, Mars, and Earth.

For Venus, the computations indicate that the greenhouse mechanism can explain the high observed surface temperature of about $700^{o}K$ if there is an extensive infrared-opaque cloud-layer at very high levels (or low temperatures) in the Venus atmosphere, as well as reasonable amounts of carbon dioxide or other infrared absorbing gases in the atmosphere. Application of the two-layer greenhouse model to the planets Mars and Earth yields predicted average surface temperatures that are within 5% of the observed average surface temperatures on these planets.

There are a number of assumptions in the two-layer greenhouse model that introduce uncertainties into the computations of the greenhouse effect on Venus. These include the assumptions of a grey atmosphere and an infrared-opaque cloud. There are also some internal atmospheric inconsistencies introduced by the model. And, finally, there is the implicit assumption that most of the solar radiation that

is not reflected by the clouds reaches the surface of the planet. Further research should be directed toward removing some of these assumptions and restrictions, or evaluating their effects.

A preliminary study has been made of the amount of solar radiation reaching the surface of Venus. In particular, the amount of solar radiation absorbed by the near-infrared bands of carbon dioxide in the Venus atmosphere has been estimated. These computations indicate that carbon dioxide absorbs about 12% of the unreflected solar radiation. Since there are presumably other absorption processes in the thick Venus atmosphere—cloud absorption and absorption by other atmospheric gases and aerosols—it may be concluded that the unreflected solar radiation is depleted by at least 12% before reaching the surface of the planet. Further research should be directed toward evaluating the other solar radiation absorption processes in the Venus atmosphere.

Under the assumption of infrared radiative equilibrium, the temperature distribution between the cloud-base and the surface of Venus has been computed. To the extent that this atmospheric layer is an infrared radiative equilibrium, and to the extent that the assumptions made in the model are realistic, the computed temperature distributions represent close approximations to the actual temperature distribution in the sub-cloud layer. Further research should be directed toward estimating the temperature profile within the clouds on the basis of reasonable assumptions of cloud composition, formation, and condensation thermodynamics.

It would be desirable to develop a physical model representing all the processes affecting the mean vertical variation of temperature in the Venus atmosphere—radiative, convective, and condensation processes—from the surface of the planet to levels above the cloud-top.

SECTION 4

LIST OF TECHNICAL REPORTS AND PAPERS PUBLISHED UNDER THE CONTRACT

A number of scientific publications has resulted from the NASA support of our research in planetary meteorology. Listed below are contract technical reports, and papers published in the scientific journals.

Contract Technical Reports:

Ohring, G., W. Tang, and G. DeSanto, 1962: Theoretical estimates of the average surface temperatures on Mars. Technical Report No. 1, Contract NASw-286, GCA Technical Report 62-3-N, 23 pp.

Ohring, G., 1962: A theoretical estimate of the average vertical distribution of temperature in the Martian atmosphere. Technical Report No. 2, Constract NASw-286, GCA Technical Report 62-7-N, 15 pp.

Ohring, G., and O. Cote', 1963: The meteorology of Mars and Venus. Annual Technical Report, Contract NASw-286, GCA Technical Report 63-6-N, 82 pp.

Ohring, G., and J. Mariano, 1963: The effect of cloudiness on a greenhouse model of the Venus atmosphere. Contract NASw-704, GCA Technical Report 63-17-N, 28 pp.

Craig, R., 1963: Tides in the atmospheres of Earth and Mars. Contract NASw-704, GCA Technical Report 63-26-N, 45 pp.

Papers Published in Scientific Journals:

Ohring, G., W. Tang, and G. DeSanto, 1962: Theoretical estimates of the average surface temperature on Mars. Journal of the Atmospheric Sciences, 19, 444-449.

Ohring, G., 1962: Theoretical estimates of the average surface and atmospheric temperature on Mars. Memoires de la Societe Royale des Sciences de Liege, 24, 425 -447.

Ohring, G., 1963: A theoretical estimate of the average vertical distribution of temperature in the Martian atmosphere. Icarus, 1, 328-333.

Ohring, G., and J. Mariano, 1964: The effect of cloudiness on a greenhouse model of the Venus atmosphere. Journal of Geophysical Research, 69, 165-175.

REFERENCES

Arking, A., 1962: Non-grey planetary atmospheres, in Proceedings of the Eleventh International Astrophysical Symposium. The Physics of the Planets, University of Liege, Belgium, pp. 180-189.

Barath, F. T., A. H. Barrett, J. Copeland, D. E. Jones, and A. E. Lilley, 1963: Mariner II: Preliminary reports on measurements of Venus - microwave radiometers. Science, 139, 908-909.

Chandrasekhar, S., 1960: Radiative Transfer. Dover Publications, New York, 393 pp.

Chase, S. C., L. D. Kaplan, and G. Neugebauer, 1963: Mariner II: Preliminary reports on measurements of Venus - Infrared radiometer. Science, 139, 907-908.

Craig, R. A., 1963: Tides in the atmospheres of Earth and Mars. GCA Technical Report No. 63-26-N, Contract NASw-704, 45 pp.

Geophysics Corporation of America, 1964: Experimental and theoretical studies in planetary aeronomy, Quart. Prog. Rept. for 15 October 1963-15 January 1964, NASw-840.

Gifford, F., 1956: The surface temperature climate of Mars. Astrophysical J., 123, 154-161.

Goody, R. M., 1954: The physics of the stratosphere. University Press, Cambridge, 187 pp.

Grandjean, R., and R. M. Goody, 1955: The concentration of carbon dioxide in the atmosphere of Mars, Astrophys. J., 121, 548-552.

Hastings, C., 1955: Approximations for Digital Computers, Princeton University Press, Princeton, 201 pp.

Holmboe, J., G. E. Forsythe, W. Gustin, 1945: Dynamic Meteorology, Wiley, New York.

Howard, J. N., D. E. Burch, and D.Williams, 1956: Infrared transmission of synthetic atmospheres II. Absorption by carbon dioxide. J. Opt. Soc. Amer., 46, 237-241.

Jastrow, R., and S. I. Rasool, 1963: Radiative transfer in the atmospheres of Venus and Mars, Space Research, Proc. Intern. Space Sci. Symp., 3rd, North-Holland Publishing Co., Amsterdam, 1036-1041.

Kaplan, L. D., 1962: A preliminary model of the Venus atmosphere. Technical Report 32-379, Jet Propulsion Laboratory, C.I.T., 5 pp.

Kaplan, L. D., G. Münch, and H. Spinrad, 1964: An analysis of the spectrum of Mars. Astrophysical J., 139, 1-15.

King, J. I. F., 1963: Private communication.

Kunz, K. S., 1957: Numerical Analysis, McGraw-Hill Book Company, Inc., New York, 381 pp.

List, R. J., 1958: Smithsonian Meteorological Tables, 6th Revised Edition, Washington, Smithsonian Institute.

London, J., 1957: A study of the atmospheric heat balance, Final Report, Contract No. AF19(122)-165, AD 117227, 99 pp.

Mariner: Mission to Venus, 1963: Prepared by the Staff, Jet Propulsion Laboratory, C. I. T., and compiled by H. J. Wheelock, McGraw Hill, New York, 118 pp.

Milankovitch, M., 1920: Theorie Mathematique des Phenomenes Thermiques Produits par la Radiation Solaire. L'Ecole Polytechnique, Paris 338 pp.

Mintz, Y., 1961: The general circulation of planetary atmospheres. Appendix 8 of the Atmospheres of Mars and Venus, NAS-NRC Publication, 944, 107-146.

Ohring, G., 1963: A theoretical estimate of the average vertical distribution of temperature in the Martian atmosphere. ICARUS, Vol. 1, 4, 328-333.

Ohring, G., W. Tang, and G. DeSanto, 1962: Theoretical estimates of the average surface temperature on Mars. J. Atmospheric Sci., 19, 444-449.

Ohring, G., and O. R. Cote', 1963: The meteorology of Mars and Venus. GCA Technical Report No. 63-6-N, Contract No. NASw-286, 82 pp.

Ohring, G., and J. Mariano, 1963: The effect of cloudiness on a greenhouse model of the Venus atmosphere. GCA Technical Report No. 63017-N, Contract NASw-704, 28 pp.

Ohring, G., and J. Mariano, 1964: The effect of cloudiness on a greenhouse model of the Venus atmosphere. Journal of Geophys. Res., 69, 165-175.

Roberts, J. A., Radio emission from the planets, Planetary Space Sci., 11, 221-260.

Sagan, C., 1960: The radiation balance of Venus, Jet Propulsion Lab. Tech. Rept. 32-34, 23 pp.

Sagan, C., 1964: Private communication.

Siebert, M., 1961: Atmospheric tides. Adv. Geophys., 7, 105-187.

Sinton, W. M., 1962: Infrared observations of Venus, in Proceedings of Eleventh International Astrophysical Symp., The Physics of the Planets. University of Liege, Belgium, 300-310.

Victor, W. K., J. Stevens, and S. W. Golumb, 1961: Radar exploration of Venus. C. I. T. Jet Prop. Lab. Tech. Rept. No. 32-132.